NASA CONTRACTOR REPORT 166467

AIRCRAFT AERODYNAMIC PREDICTION METHOD FOR V/STOL TRANSITION INCLUDING FLOW SEPARATION

B. R. Gilmer

G. A. Miner

D. R. Bristow

CONTRACT NAS2–11161
April 1983

NASA

NASA CONTRACTOR REPORT 166467

AIRCRAFT AERODYNAMIC PREDICTION METHOD FOR V/STOL TRANSITION INCLUDING FLOW SEPARATION

B. R. Gilmer

G. A. Miner

D. R. Bristow

McDonnell Douglas Corporation
Saint Louis, Missouri

Prepared for

Ames Research Center
Under Contract NAS2-11161

National Aeronautics and
Space Administration

Ames Research Center
Moffett Field, California 94035

SUMMARY

A numerical procedure has been developed for the aerodynamic force and moment analysis of V/STOL aircraft operating in the transition regime between hover and conventional forward flight. The procedure specifically treats the interaction between the jets and airframe as well as the effect of turbulent flow separation on the wing and plain wing trailing edge devices. The overall methodology employs three previously existing computer programs for the calculation of the jet properties and inviscid parameters, plus a newly developed method for predicting wing viscous effects.

The trajectories, cross sectional area variations, and mass entrainment rates of the jets are calculated by the Adler-Baron Jet-in-Crossflow Program. The inviscid effects of the interaction between the jets and airframe on the aerodynamic properties are determined by use of the MCAIR 3-D Subsonic Potential Flow Program, a surface panel method. In addition, the MCAIR 3-D Geometry Influence Coefficient Program is used to calculate a matrix of partial derivatives that represent the rate of change of the inviscid aerodynamic properties with respect to arbitrary changes in the effective wing shape.

For each baseline configuration, the calculated quantities from the second and third programs above establish an input file to the MCAIR Stalled Wing Analysis Program (SWAP). The purpose

of SWAP is to calculate the surface pressure distribution, forces and moments on the aircraft in the presence of wing viscous effects including turbulent flow separation on the wing and unslotted wing trailing edge devices. The viscous-inviscid interaction is explicitly modelled by a first order coupling between mathematical expansions of the inviscid and viscous flow methods. SWAP can be employed for wing alone geometries, wing-fuselage combinations, as well as wing-fuselage-jet configurations.

The complete calculation procedure is described with mathematical formulations presented for the Stalled Wing Analysis Program. Example solutions are presented that demonstrate the accuracy, numerical stability, and efficiency of the jet-aircraft-viscous interaction methodology.

TABLE OF CONTENTS

LIST OF ILLUSTRATIONS

LIST OF ILLUSTRATIONS

LIST OF ILLUSTRATIONS

LIST OF TABLES

LIST OF SYMBOLS

A_{1k}	Matrix of terms representing first order rate of change in chordwise tangential edge velocity with respect to change in geometric unknowns
a_1, a_2, a_3, a_4	Coefficients of cubic polynomial for Z
B_{1k}	Matrix of terms representing first order rate of change in spanwise tangential edge velocity with respect to change in geometric unknowns
b	Length of wing span
b_1, b_2, b_3, b_4, b_5	Coefficients of cubic polynomial for U
C	Reference chord length
C_D, C_L, C_M	Configuration drag, lift, and pitching moment coefficients
C_N	Configuration normal force coefficient
C_d, C_l, C_m	Section drag, lift, and pitching moment coefficients
C_f	Skin friction coefficient
C_p	Pressure coefficient
C_{kj}	Matrix of linear equation coefficients
C_{1k}	Matrix of terms representing first order rate of change in boundary layer displacement thickness with respect to change in geometric unknowns
D	Diameter of jet at exit conditions
D_{1k}	Matrix of terms representing first order rate of change in boundary layer main flow shape factor with respect to change in geometric unknowns
E_{ik}	Matrix of terms representing first order rate of change of error with respect to change in geometric unknowns
F	Least squares error function
f	Function
g_k	Independent geometric unknown vector
H	Main flow boundary layer shape factor

LIST OF SYMBOLS

h_1, h_2, h_3	Metric coefficients
M	Mach number
$\dot{m}$	Mass entrainment rate
$\dot{m}_o$	Mass flow out of jet nozzle
N	Normal vector
NKS	Number of independent panel cornerpoint perturbations
NSPANI	Number of independent span stations on wing
N_{unk}	Number of independent geometric unknowns
P	Viscous region index
R_∞	Freestream Reynolds Number Based on Reference Chord
R_{ns}	Crossflow boundary layer thickness Reynolds number
R_T	Mainflow momentum thickness Reynolds number at transition point
R_{TT}	Critical mainflow momentum thickness Reynolds number for transition
R_X	Surface distance Reynolds number
RHS	Right hand side of equation
T_E	Mainflow momentum thickness
t	Thickness
U	Tangential edge velocity magnitude in chordwise direction
V	Tangential edge velocity magnitude in spanwise direction
W	Inviscid velocity
WT	Least squares weight
X,Y,Z	Cartesian coordinates
X',Y',Z'	Boundary layer coordinates

LIST OF SYMBOLS

α	Angle of Attack
β	Boundary layer limiting wall streamline angle
γ	Angle between X' axis and projection of external streamline onto wing surface.
ε	Error between desired and actual conditions of theoretical model for wing effective shape
η	Fraction of wing semi-span
θ	Angle
θ'	Instantaneous angle between wing effective shape and baseline shape
λ	Angle between X' and Y' axes
Λ	Leading edge sweep angle
τ_ω	Viscous shear stress at wing surface
ϕ	Velocity potential

Subscripts

A	First point in viscous region
AERO	Aerodynamic
ATTCH	Attachment line
B	Last point in viscous region
D	Discontinous
E	Endpoint
J	Jet
L	Lower
lwr	Lower
M	Midpoint
S	Separation point
SEP	Separation point

LIST OF SYBOLS

TE	Trailing edge
TOT	Total
TR	Transition point
U	Upper
upr	Upper
V	Viscous coordinate
WTE	Wake trailing edge
X,Y,Z	X, Y, and Z gradients or directions
∞	Freestream

INTRODUCTION

An automated method is presented for predicting the aerodynamic performance of complete V/STOL aircraft operating out of ground effect in the transition regime between hover and conventional forward flight. In transition, the large jet injection angles, low aircraft velocity, relatively low Reynolds number, and high trailing edge flap deflections lead to strong viscous aerodynamic-propulsion interactions that have a substantial effect on aircraft forces and moments (Figure 1).

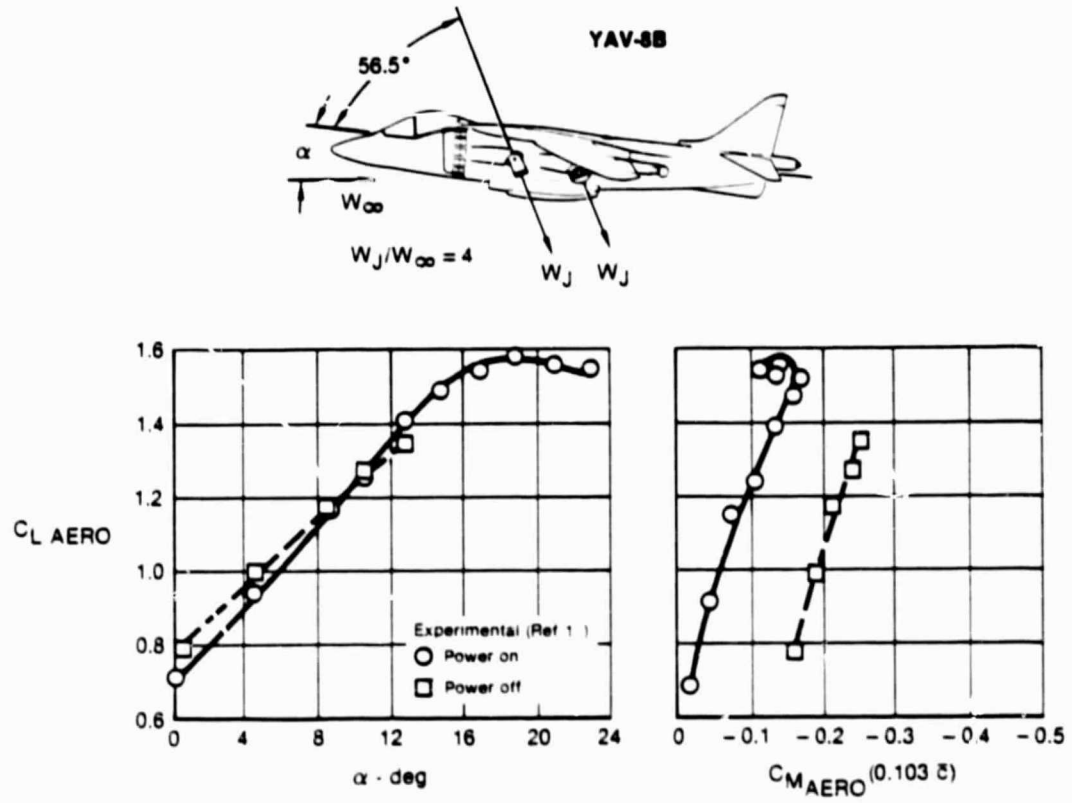

FIGURE 1. V/STOL TRANSITION: EFFECT OF JETS ON AERODYNAMIC FORCE AND MOMENT

The specific flow phenomena that produce these large interactions are presented in Figure 2. Although the blockage and mass entrainment of the jets have a substantial effect on the surrounding aerodynamic flow field, the effect of the airframe on the properties of the jets-in-crossflow is typically very weak. This fact allows the jet centerline trajectory, cross-section geometry, and entrainment rate to be calculated by an independent (decoupled) jet-in-crossflow method.

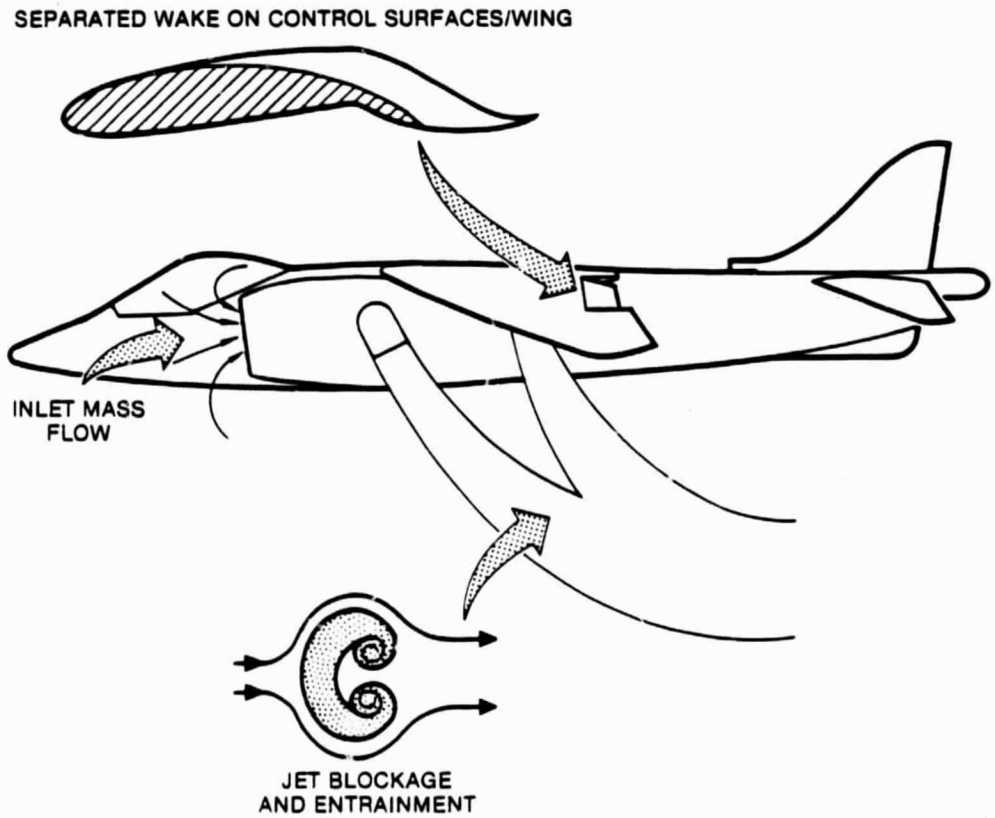

FIGURE 2. PROBLEM DESCRIPTION: V/STOL TRANSITION FLOW FIELD

If the surrounding aerodynamic flow field were incompressible and inviscid, a surface panel method could be applied to calculate the induced forces and moments on the airframe surface (Reference 2). Panelled jets with surface suction would represent the effects of jet blockage and entrainment. However, in the transition mode there can be large regions of separated flow associated with highly deflected control surfaces or high angles-of-attack. Panel methods are appropriate for analyzing the flow in the presence of regions of separation if the panelled geometry includes the viscous displacement surface. The problem is to solve for the displaced surface; the difficulty is that the solution is dependent upon strong viscous-inviscid interactions.

In the past decade several methods have been developed for predicting the incompressible aerodynamic forces and moments of two dimensional airfoils in the presence of turbulent flow separatio (References 3-7). Most of these methods empirically model the turbulent flow separation region by constant pressure from the separation point to the airfoil trailing edge with some method for closing off the wake downstream. This bypasses the need to perform complex computations within the viscous separated flow region. An inverse two-dimensional potential flow method is used to "design" the streamline contour that satisfies the constant pressure conditions on the separated wake.

With the development of three-dimensional wing inverse potential flow (or design) methods (References 8-11), the expectation

was that finite wing viscous-inviscid interactions including turbulent flow separation would be forthcoming. However, reliable methods had not been developed for several reasons. First, most of the two dimensional viscous-inviscid interaction procedures utilize simple iteration between distinct viscous-only and inviscid-only calculation steps. This procedure can be numerically unstable and often requires man-in-the-loop corrections to insure accuracy and numerical stability. Second, accurate three-dimensional conventional panel methods and design methods are expensive to use. Iterating between a panel method, a viscous calculation method, and a design method for five or more iterations for each angle-of-attack can be prohibitively expensive. Third, until recently the design methods suffered from numerical instabilities that precluded the accurate and efficient coupling to viscous methods. All of these difficulties should be dealt with simultaneously when considering the finite wing viscous-inviscid interaction problem.

Three recent advances have overcome the major difficulties with three dimensional viscous-inviscid interaction predictions. In 1980 the McDonnell Aircraft Company (MCAIR) Stalled Airfoil Analysis Program (Reference 7) was developed for the reliable prediction of 2-D airfoil forces and moments in fully attached or turbulent separated flow In 1981, the MCAIR 3-D Perturbation Analysis Method (Reference 12) was developed under contract to NASA, Langley Research Center, for the accurate and inexpensive

inviscid solution corresponding to arbitrary small perturbations to wing-fuselage geometries. In 1982, the MCAIR 3-D Subsonic Wing Design Program (Reference 11) was developed under contract to NASA, Langley Research Center, for the accurate, inexpensive, numerically stable design of wing-on-fuselage geometries corresponding to prescribed pressure distributions.

This report presents a method developed at MCAIR for the analysis of jet-airframe wing viscous-inviscid interactions including turbulent flow separation on the wing or plain wing trailing edge devices. The method, the Jet-Aircraft-Viscous Interaction (JAVI) Program, represents the synthesis of the three advances that make possible accurate, numerically stable solutions to the 3-D viscous flow problem. Furthermore, by incorporating complex aircraft configurations through the use of the panel method, the approach is applicable to wings, wing-fuselage combinations, and wing-fuselage-jet configurations.

This report presents the complete calculation procedure for treating jet, airframe, and wing viscous interactions. The four different computer programs employed are discussed. Mathematical formulations for the wing viscous-inviscid interaction analysis are presented with example solutions that demonstrate the accuracy and stability of the method. Conclusions and recommendations are presented.

CALCULATION PROCEDURE FOR JET-AIRFRAME-VISCOUS INTERACTIONS

The computation of the aerodynamic performance of V/STOL aircraft in transition out of ground effect requires the use of four computer programs:

(a) Adler-Baron Jet-In-Crossflow Program (JICP; Ref 13)

(b) MCAIR 3-D Subsonic Potential Flow Program (SPFP; Ref 12)

(c) MCAIR 3-D Geometry Influence Coefficient Program (GICP; Ref 12)

(d) MCAIR 3-D Stalled Wing Analysis Program (SWAP)

It is assumed the the flow is incompressible and that the following quantities are known: (1) airframe geometry, (2) the freestream angle of attack and unit Reynolds number, (3) the engine inlet mass flow, and (4) uniform nozzle exit conditions (injection angle and jet to freestream velocity ratio). Furthermore, it is assumed that the jets are incompressible and turbulent, and any trailing edge device is unslotted.

The calculation procedure is depicted in Figure 3. The first step is to determine the jet properties under the assumption that airframe influence on the jets is negligible. Each jet injection angle, θ_J, and jet-to-freestream velocity ratio, $\frac{W_J}{W_\infty}$, are converted by JICP to jet centerline trajectory, cross sectional geometry, and mass entrainment rate. The jet geometry is

panelled and connected to a panelled representation of the baseline aircraft geometry (aircraft without viscous displacement thickness). The mass entrainment of the jet is represented by suction distributed over the jet panels.

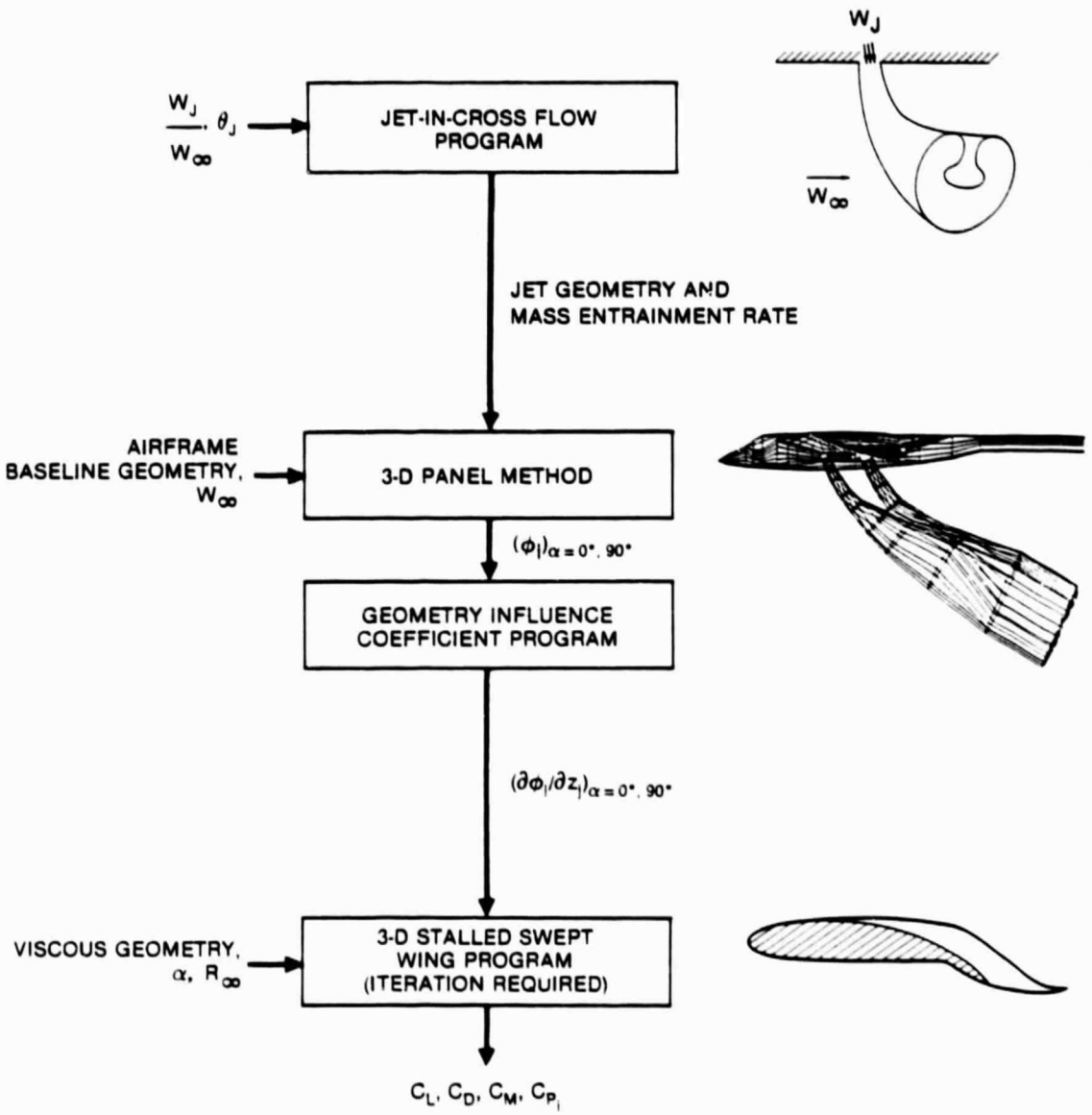

FIGURE 3. CONFIGURATION VISCOUS-INVISCID ANALYSIS PROCEDURE

The baseline configuration is converted to a distribution of inviscid surface pressure and an aerodynamic influence coefficient matrix by SPFP. The output from this program is used as input to GICP, which calculates a matrix of partial derivatives. Each element of this matrix represents the rate of change of the inviscid perturbation potential on the surface with respect to arbitrary changes in the wing displacement. GICP is executed twice corresponding to angles-of-attack of zero and ninety degrees.

The output from SPFP and GICP are used as input files to SWAP, which uses the inviscid perturbation matrices from GICP to extrapolate for the pressure solution corresponding to the desired angle-of-attack and calculated wing displacement surface. The wing effective shape is determined iteratively along with the distribution of pressure over the aircraft surface. Forces and moments are determined by integration of pressure over the aircraft and surface shear stress over the wing.

The remainder of this section is devoted to a description of the four programs. More detailed descriptions of the first three programs are available in the literature (References 12 and 13), and the mathematical formulation for SWAP is presented in the next section.

Jet-In-Crossflow Program

The Adler-Baron Jet-In-Crossflow Program (Reference 13) converts the jet injection angle and jet-to-freestream velocity ratio to the jet centerline trajectory, cross-sectional area variation, and mass entrainment rate. The method is applicable to incompressible turbulent jets and is based on two integral momentum equations. One of these is in the direction perpendicular to the jet centerline, and the other is in the direction parallel to the jet centerline. The mass entrainment rate, needed to solve these equations, is based on a linear combination of straight jet entrainment (no crossflow) and vortex pair entrainment. Integration of the two momentum equations along the jet centerline requires a knowledge of the velocity distribution over the jet cross section. The contour of jet velocity at the boundary between the jet and freestream is determined by calculating the displacement of two-dimensional vortices initially seeded on the nozzle exit. The vortices simulate the shear layer between the jet and surrounding flow. The inner contours of progressively higher velocity are generated by solving Poisson's equation, which is an empirical mathematical model. A detailed discussion of the procedure is found in Reference 13.

The Jet-In-Crossflow Program is restricted to one isolated jet issuing from a flat plate into freestream. Due to the weak effect of the airframe on the jet, it is reasonable to calculate

the jet properties in isolation. For multiple jets, the program is executed once for each jet. Furthermore, for tandem jets, as is the case for the YAV-8B, the upstream jet exerts a large influence on the downstream one, and the jets tend to coalesce. For multiple jets with interaction and coalescence, the method of Wooler (Reference 14) is used to determine the blockage effects of the upstream jet on the downstream jet. The merged single jet properties are determined to a first approximation by simply combining the effects of the individual jets without coalescence.

A demonstration of the accuracy of JICP is shown in Figures 4-6, where the predicted jet centerline trajectory, cross-sectional area ratio, and entrained mass flux are compared with experiments (Reference 15). The agreement is good for the cases examined.

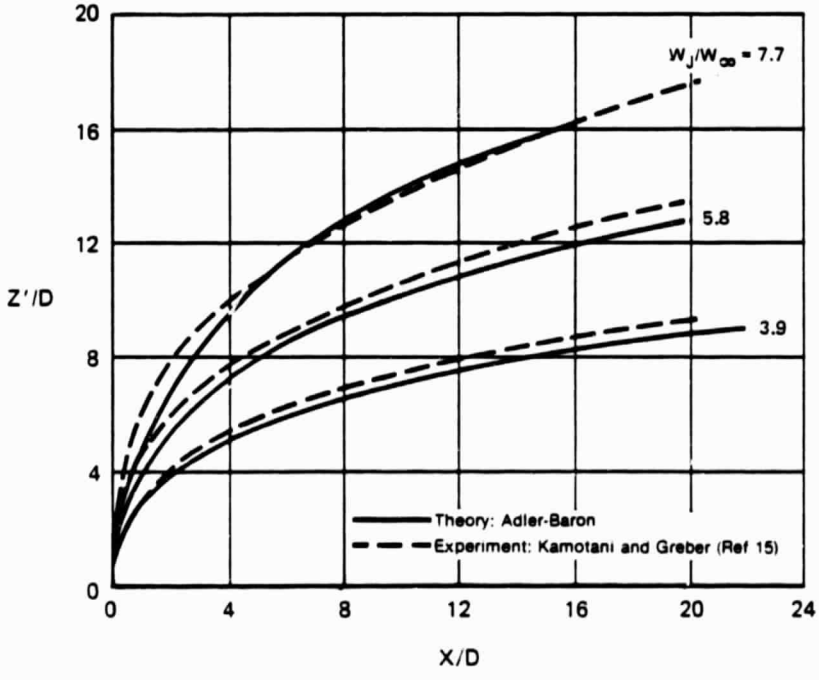

FIGURE 4. LOCUS OF PEAK JET VELOCITY CENTERLINE TRAJECTORY
90° INJECTION ANGLE

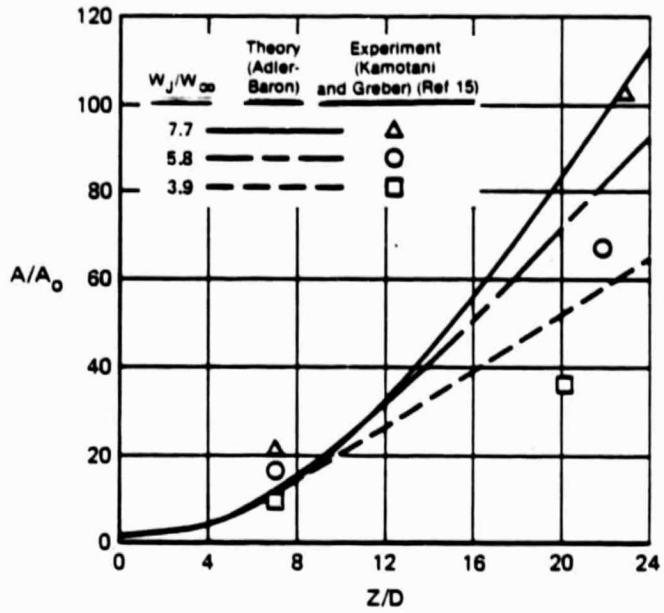

FIGURE 5. JET CROSS-SECTIONAL AREA RATIO COMPARISON
90° INJECTION ANGLE

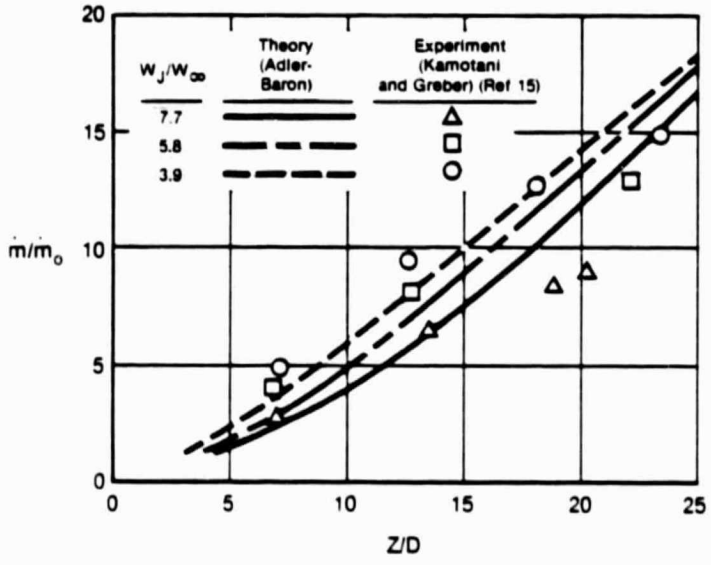

FIGURE 6. ENTRAINED MASS FLUX COMPARISON
90° INJECTION ANGLE

Subsonic Potential Flow Program

The MCAIR 3-D Subsonic Potential Flow Program (Reference 12) is a surface panel method that is based on the combined source-doublet distribution of the classical third identity of Green (Reference 16). The advantages of this combined source-doublet distribution for a surface panel method are well documented (Reference 17). The mathematical formulation employs a constant source distribution and a quadratic doublet distribution on each panel, where the solution singularity strengths are determined by satisfying indirect internal perturbation potential boundary conditions (Reference 18). The flow velocity on each panel is then established from local velocity-singularity relationships associated with Green's third identity, instead of direct summation of the influences of the singularities on all the panels. The method is formulated with a Göthert type compressibility correction; however, this option is not used in the present method. A detailed discussion of the method is found in Reference 12.

This panel method is used to calculate the airframe inviscid pressure distribution induced by the aircraft forward velocity plus the blockage and mass entrainment effects of the jets. A demonstration of the accuracy of the panel method is presented in Figure 7, where the YAV-8B wing pressure distribution in conventional flight (.50 M_∞ , 6.4° angle-of-attack) is compared to wind tunnel data (Reference 1). The ability of the panel method to

model geometric details is reflected in the accuracy of the lower surface pressures at 25% semispan, where the effect of the protruding nozzles is substantial. Wind tunnel surface pressure data for the YAV-8B in V/STOL transition is not available for comparison with analytical predictions; however, detailed pressure data are available for a single circular jet emanating from a flat plate into a uniform crossflow (Reference 19). In Figure 8, the geometry for the panelled jet was calculated by the Adler-Baron method. In the surface panel method, the effect of the mass entrainment is simulated by distributed normal velocities on the jet panel surfaces. The pressure distribution on the plate calculated by the panel method agrees well with experimental data, except in the wake of the jet (Figure 9). Although the separated wake of a jet-in-crossflow represents an important aerodynamic problem that requires further investigation, it is beyond the scope of the present effort. The good agreement for this jet-plate combination demonstrates that the treatment of the jet decoupled from plate is satisfactory.

Geometry Influence Coefficient Program

The formulation for this program is similar to the conventional panel method with one major exception. In each step of the solution process, the derivative of each quantity with respect to geometric coordinates is established, rather than the quantity itself. This process culminates in the generation of a

matrix of partial derivatives of potential with respect to arbitrary geometric perturbations. The complete mathematical formulation is described in Reference 12.

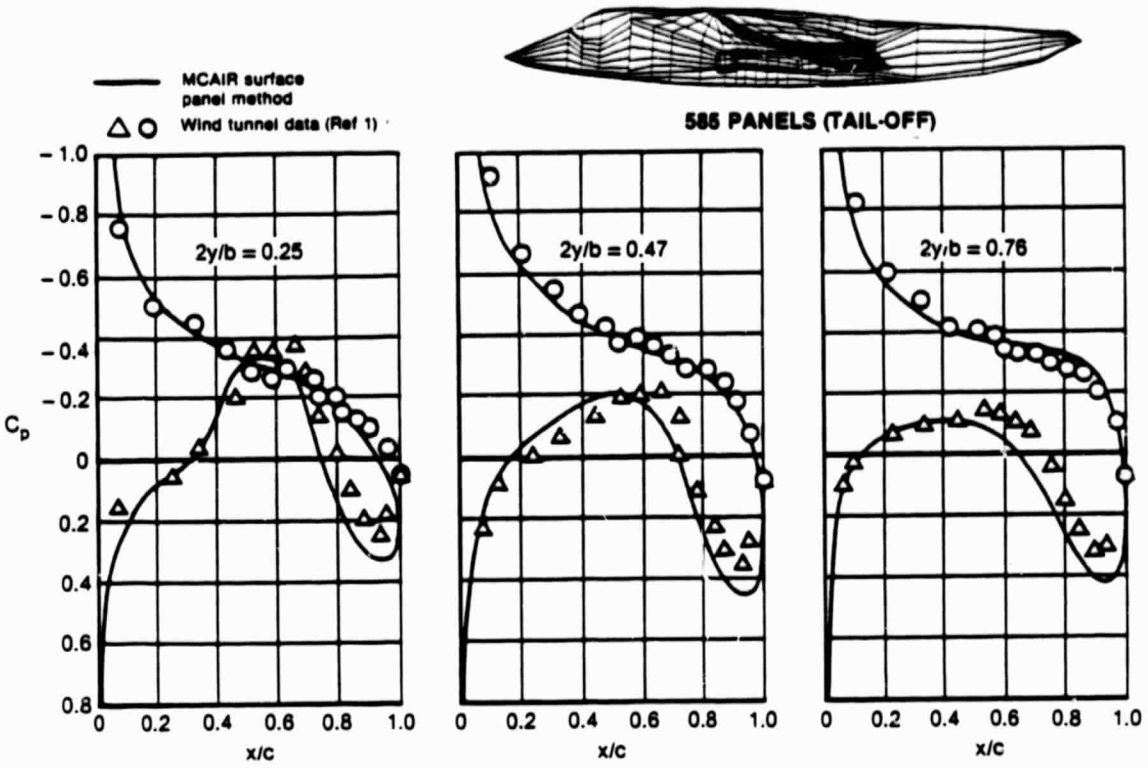

FIGURE 7. YAV-8B AT 6.4° ANGLE-OF-ATTACK IN CRUISE MODE
$M_\infty = 0.50$

The purpose of establishing the inviscid perturbation matrix is to eliminate the repetition of computationally expensive steps corresponding to a series of small arbitrary geometry perturbations to a given baseline configuration. By running this program twice at angles-of-attack of zero and ninety degrees and using an automated extrapolation procedure incorporated in SWAP, the distribution of surface pressure, corresponding to arbitrary angle-of-attack and small geometry perturbations to the baseline, can

be calculated at small expense. The method is very accurate for large changes in wing camber and twist, characteristic of wing viscous displacement effects. This extrapolation procedure is called the Perturbation Analysis Method (Reference 12).

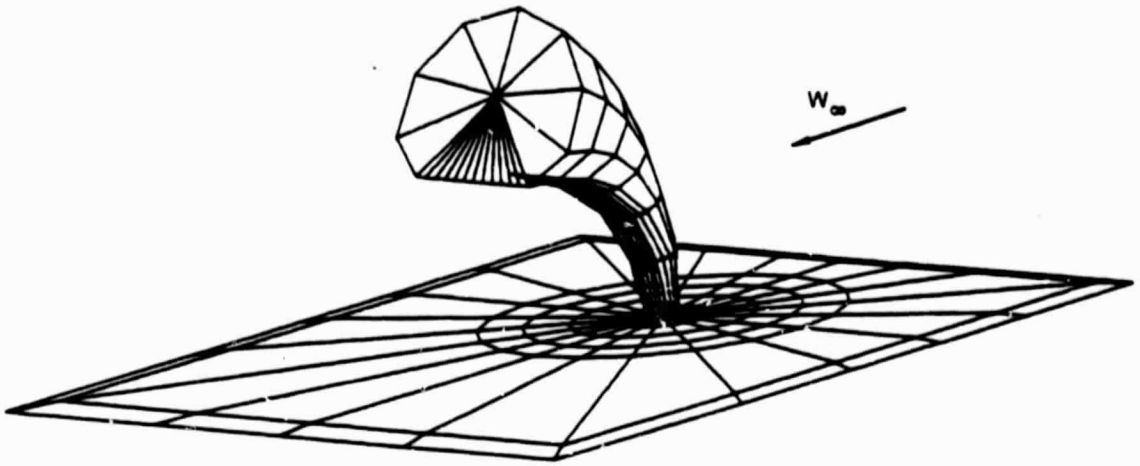

FIGURE 8. PANELING FOR A FLAT PLATE AND CIRCULAR JET-IN-CROSSFLOW
$W_J/W_\infty = 7 \quad \theta = 90°$

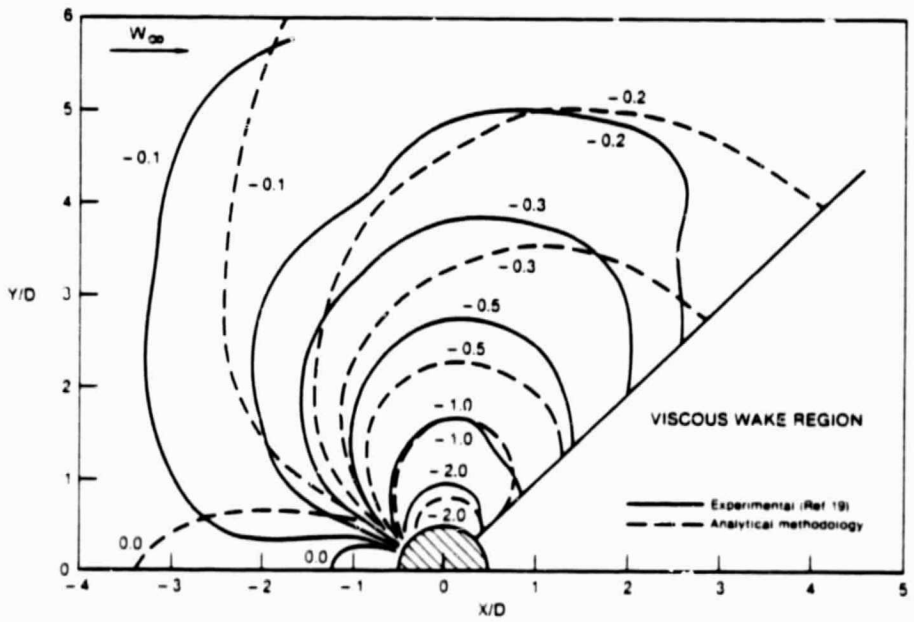

FIGURE 9. INDUCED PRESSURE DISTRIBUTION COMPARISON
$W_J/W_\infty = 7 \quad \theta = 90°$

As illustrated in Figures 10-15, the Perturbation Analysis Method is accurate for surprisingly large geometry perturbations. The low aspect ratio wing of Figure 10 with constant NACA 0012 section geometry was selected as a baseline panelled configuration. The section geometry was then perturbed twice, first to form a supercritical wing and second to form a fighter wing (Figure 11). Computed results for the perturbed geometries (Figures 12-15) are nearly identical to the virtually exact solutions obtained using a conventional surface panel method, but the computing expense is more than an order of magnitude less.

Stalled Wing Analysis Program

The objective of the Stalled Wing Analysis Program is to determine the wing effective shape (viscous displacement surface) and the resulting distribution of surface pressure over the aircraft. JICP and SPFP are each executed once for each case to be analyzed. GICP is executed twice. The data needed to run SWAP are stored as permanent input files. The analysis of the geometry over a range of angles-of-attack and different Reynolds numbers may be then accomplished by SWAP without having to rerun any of the first three computer programs.

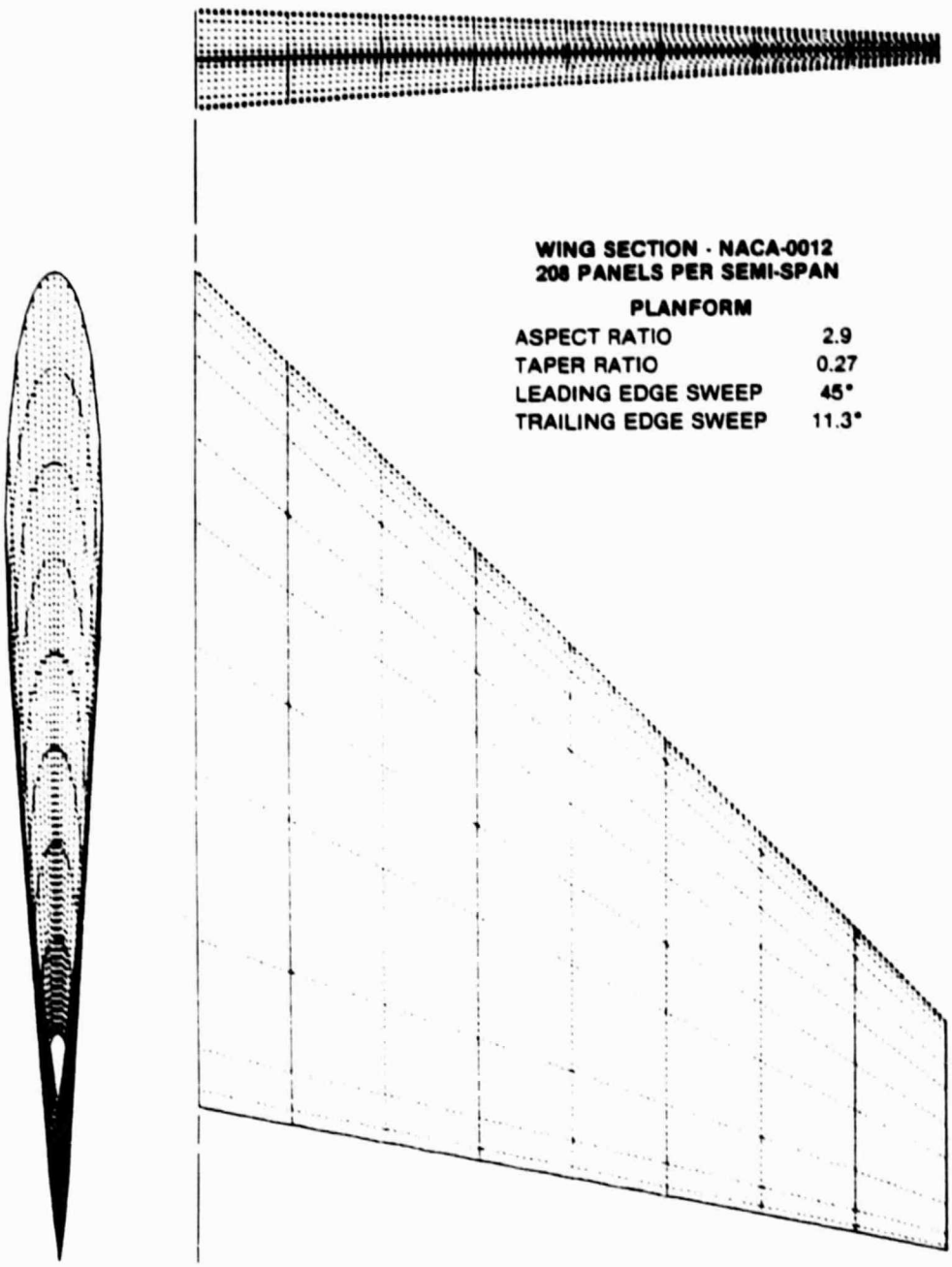

FIGURE 10. BASELINE WING PANELING FOR DEMONSTRATION OF PERTURBATION ANALYSIS METHOD

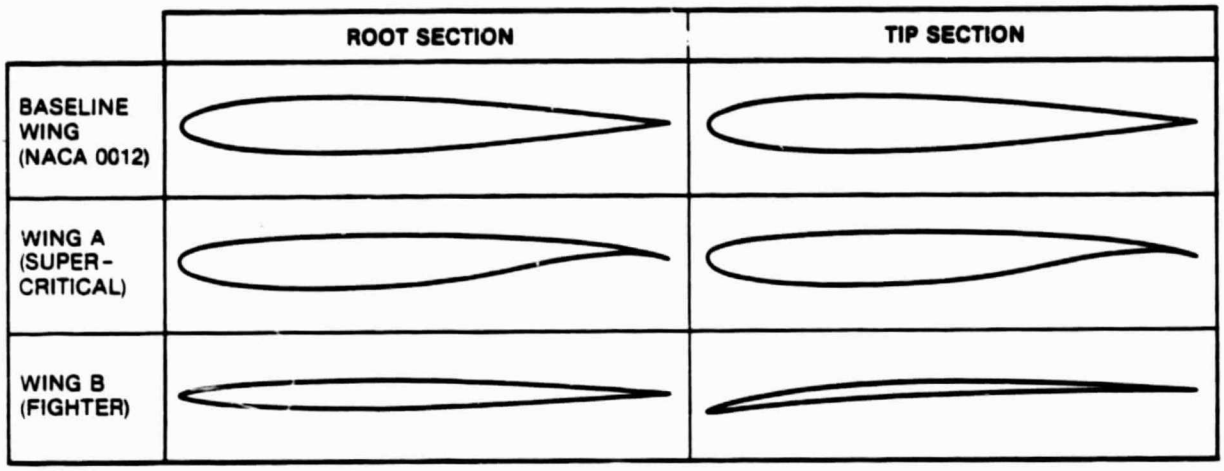

FIGURE 11. TEST CASES FOR THE PERTURBATION ANALYSIS METHOD

The procedure in SWAP is to (1) extrapolate the inviscid pressure distribution for the angle-of-attack and latest estimate for the wing effective shape, (2) calculate the viscous flow parameters and the difference between the desired conditions that define the wing effective shape and the actual calculations, (3) linearly couple the inviscid and viscous parameters to determine the changes in the effective shape necessary to simultaneously satisfy the desired conditions to first order, (4) update the effective shape, and (5) repeat steps (1) through (4) to convergence. The forces and moments are determined by integration of pressure over the aircraft surface and wall shear stress over the wing. The mathematical formulation and example solutions are presented in the next two sections.

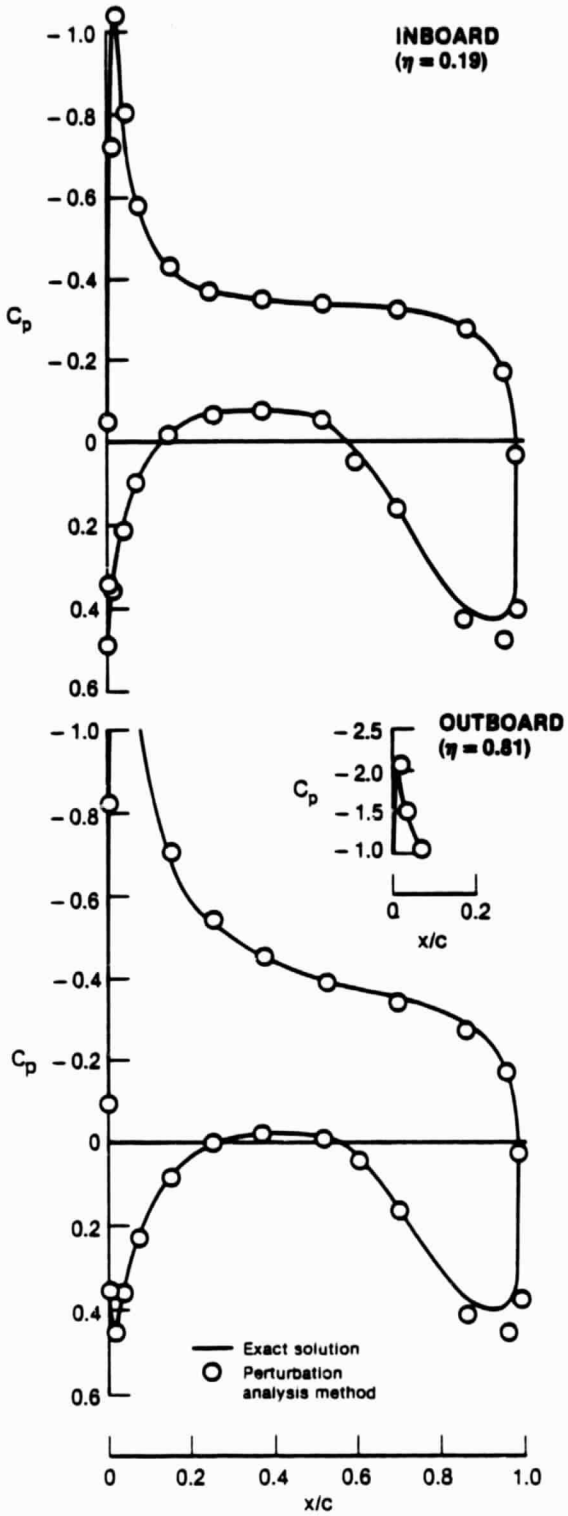

FIGURE 12. PRESSURE DISTRIBUTION OF WING A AT 5° ANGLE-OF-ATTACK SUPERCRITICAL

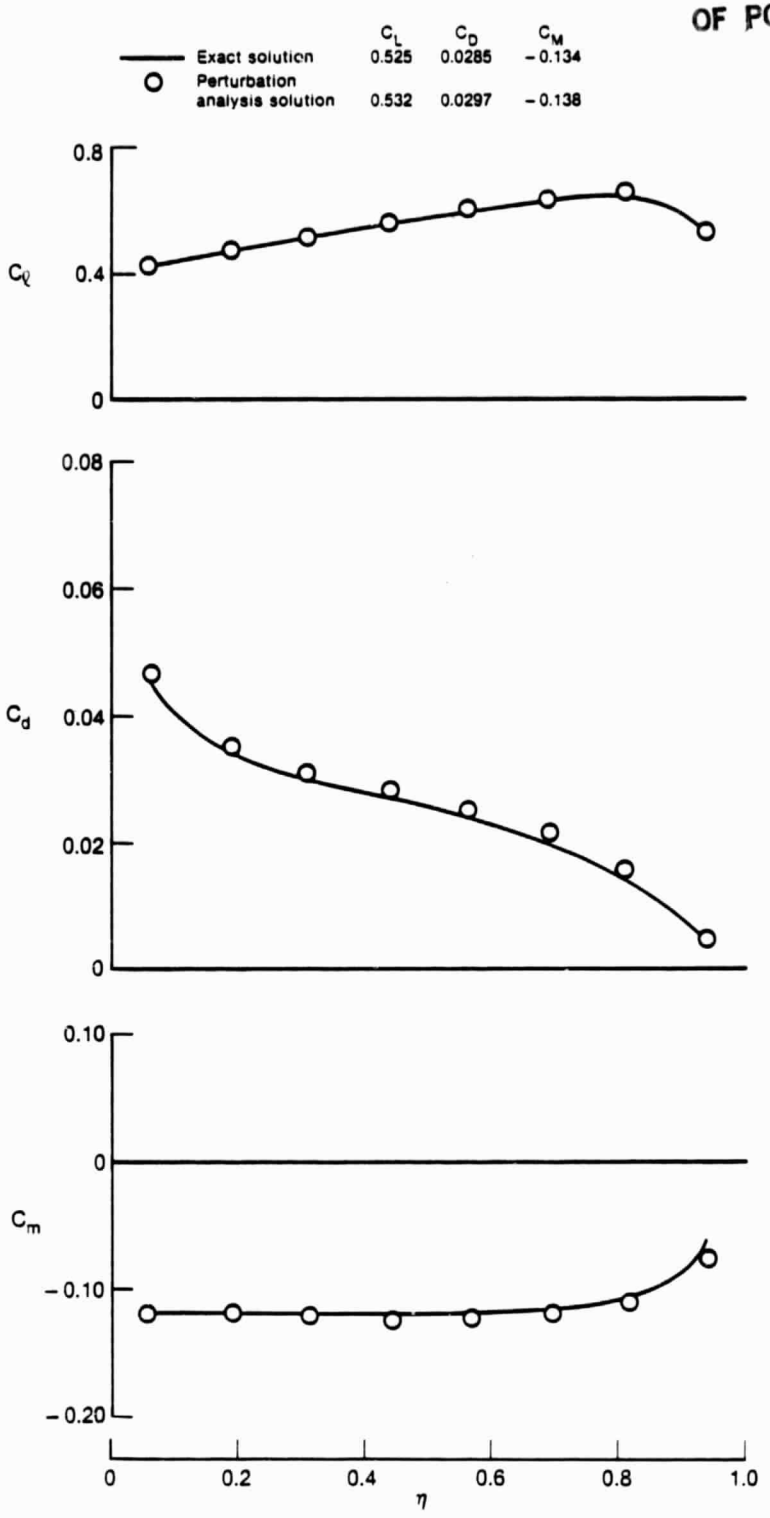

FIGURE 13. FORCE AND MOMENT DISTRIBUTION OF WING A AT 5° ANGLE-OF-ATTACK SUPERCRITICAL

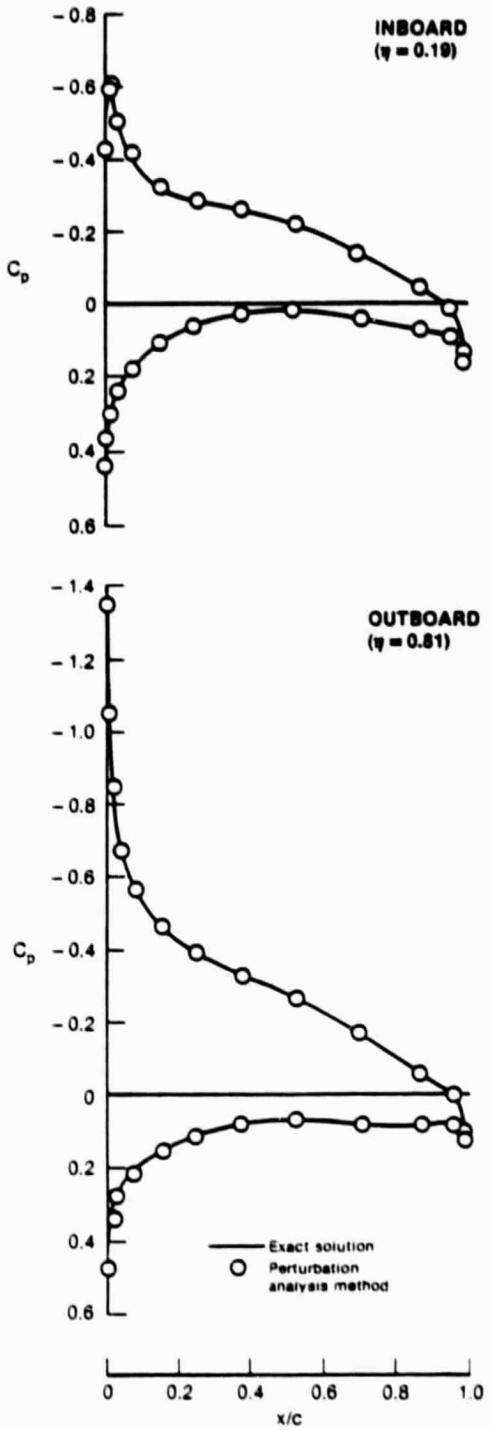

FIGURE 14. PRESSURE DISTRIBUTION OF WING B AT 5° ANGLE-OF-ATTACK
FIGHTER

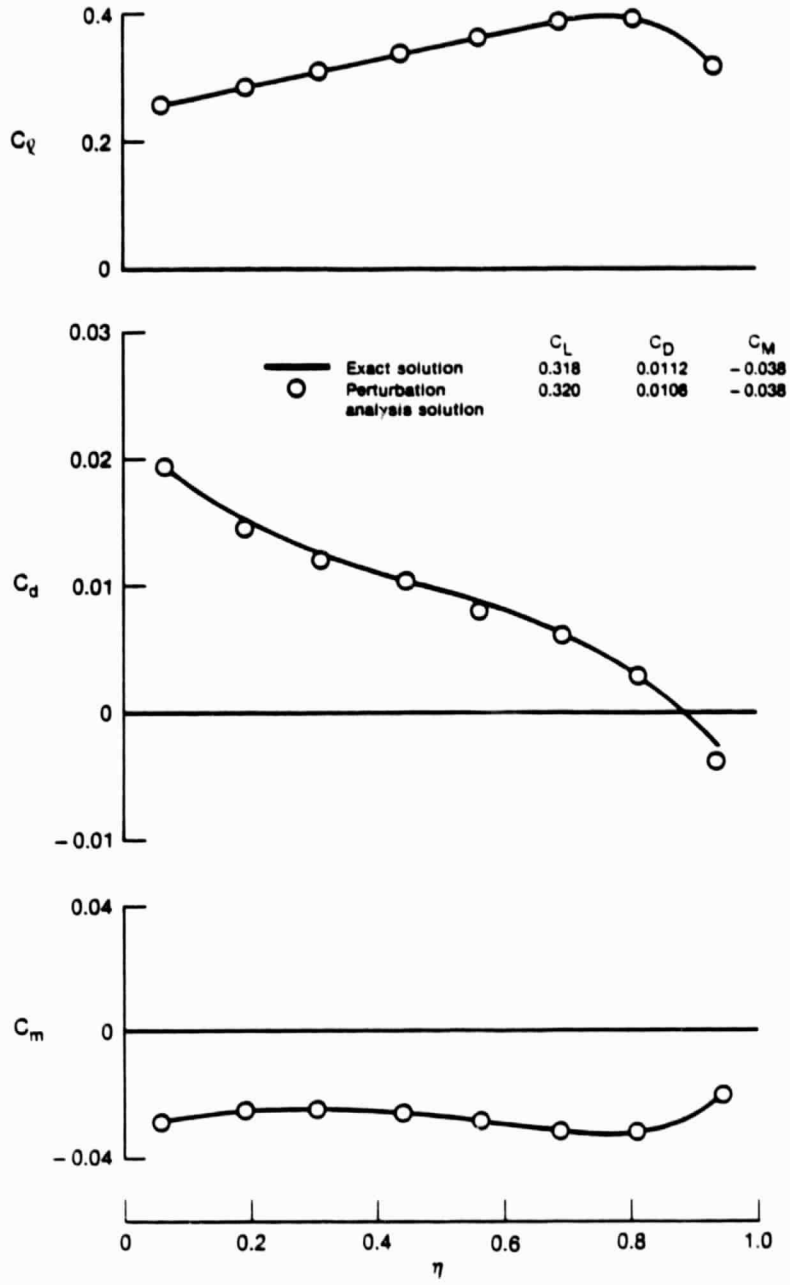

FIGURE 15. FORCE AND MOMENT DISTRIBUTION OF WING B AT 5° ANGLE-OF-ATTACK FIGHTER

SWAP is operational on the MDC Cyber 175 and is accurate and reliable for fully attached flow. The method requires further development for separated flows as expected reliability has not been achieved. Prediction at angles-of-attack below maximum lift are satisfactory; however, as maximum lift angle-of-attack is approached, the method has difficulties with both convergence and accuracy. These problems are being investigated with solutions expected in the near future.

MATHEMATICAL FORMULATION FOR STALLED WING ANALYSIS PROGRAM

The Stalled Wing Analysis Program (SWAP) is formulated to allow for turbulent separation on the wing and one full span plain wing trailing edge device. Short bubble type laminar separation is allowed and is treated as the point of transition to turbulence. Long bubble laminar separation or bubble burst is not treated.

The method is based on the hypothesis that there exists a viscous displacement surface (wing effective shape) on which the pressures calculated by potential theory agree with the viscous pressures on the surface of the wing. The formulation requires (1) a set of conditions, called the theoretical model, that specify this displacement surface, (2) numerical methods for determining the surface pressure and boundary layer growth, (3) a specialized, discretized representation of the geometry and (4) a calculation procedure for determining the geometry that satisfies the theoretical model. Each of these topics is discussed.

Theoretical Model for Wing Effective Shape

The set of conditions that specify the wing effective shape is depicted in Figure 16. The viscous displacement of the laminar boundary layer and the forward half of the length of the turbulent boundary layer on both upper and lower surfaces is neglected. The transition of the boundary layer from laminar to turbulent flow is considered instantaneous and is determined from one of three empirical correlations for mainflow transition, crossflow transition, and laminar separation. For the aft half of turbulent attached flow, the effective wing shape is the conventional representation of the wing plus boundary layer displacement thickness, δ^*. The location of the turbulent separation line is based on a critical value of the mainflow boundary layer shape factor, H, which is representative of vanishing wall shear stress in the mainflow direction.

The separated viscous wake model is based on empirical observations. First, the pressure within the separation region along the wing surface in the chordwise direction is approximately constant. Downstream of the wing trailing edge, the viscous wake is divided into two regions, referred to as the fore and aft trailing viscous wakes. The fore wake is allowed to have thickness and camber, whereas the aft wake is very thin having only camber. The wake camber line is specified by the condition that the wake cannot support a force, $\Delta C_p = 0$. The thickness distribution in the fore wake is determined by requiring the

chordwise pressure recovery on this surface to be linear from the value at the wing trailing edge to approximately freestream at the end of the fore wake.

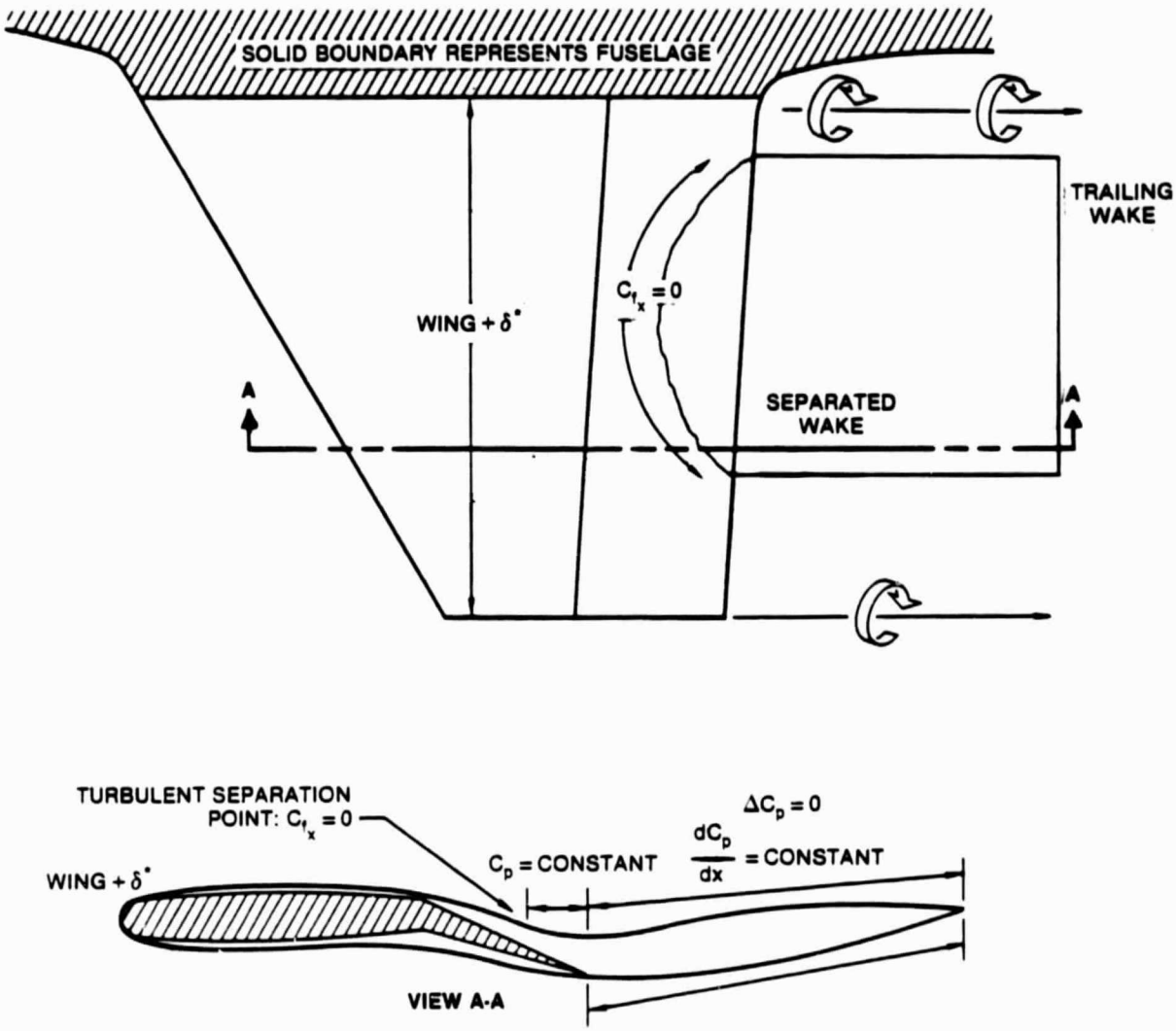

FIGURE 16. THEORETICAL MODEL FOR VISCOUS-INVISCID INTERACTIONS

The inviscid trailing wake is modelled as a sheet of constant streamwise vorticity extending far downstream. The effect of the roll up of the flap and wing tip vortices is considered to be small compared to the effect of viscous separation and is not modelled.

Selected Numerical Methods

The numerical methods were selected based on accuracy and numerical stability. As mentioned in the previous section, the pressure solution is determined by incorporating the logic of the Perturbation Analysis Method (Reference 12). In addition to the accuracy and efficiency previously discussed, this method offered the advantage of providing a mathematical formulation for calculating a matrix, whose elements correspond to the rate of change in the velocity at each panel center with respect to arbitrary displacements to the panel cornerpoints. This matrix is necessary to linearly couple the inviscid and viscous conditions of the theoretical model.

The selected methods for determining the boundary layer growth on the wing surface are depicted in Figure 17. Along the attachment line, the laminar flow, transition, and turbulent flow are predicted by the methods due to Rosenhead, Pfenninger, and Smith (References 20, 21, and 22), respectively. The laminar flow characteristics are predicted by the Cooke method (Reference 23). Mainflow and crossflow transition are determined by

empirical correlations due to Michel (Reference 24) and Gross (Reference 25). The turbulent flow characteristics are predicted by the method due to Smith (Reference 26). The separation location is determined by the mainflow shape factor exceeding a value of 2.0.

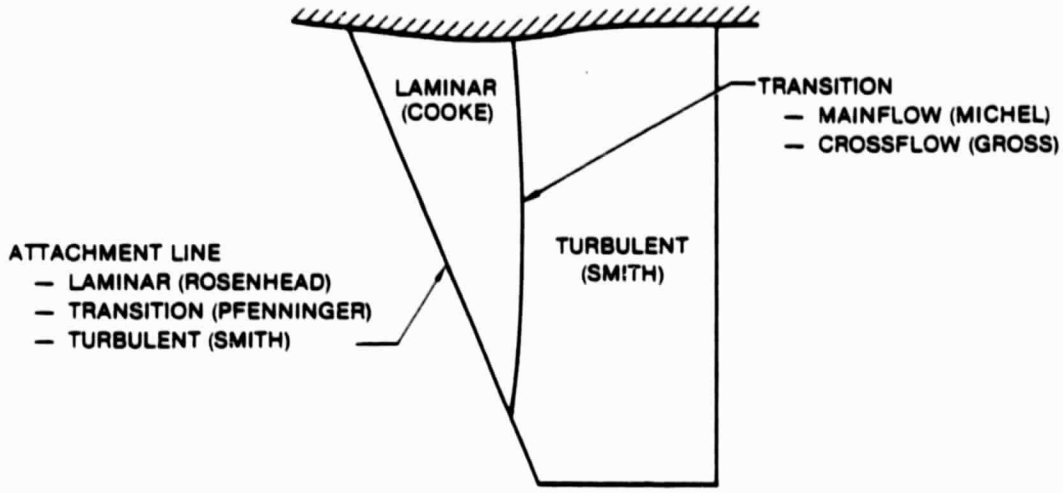

FIGURE 17. SELECTED BOUNDARY LAYER METHODS

All of these methods are integral boundary layer methods, or, in the case of the transition prediction methods, analytical representations of empirical curve fits. The empirical curve fits were selected primarily because efficient, accurate, analytical methods are not available for predicting three-dimensional transition. The integral boundary layer methods were selected for their accuracy and numerical stability. While not as accurate as finite difference methods in predicting detailed boundary layer parameters, the integral methods are entirely sufficient for calculating the global effects of viscous-inviscid interactions on the total forces and moments.

Geometric Representation of Wing Effective Shape

A right-handed Cartesian coordinate system is employed by the inviscid calculation methods. X is taken in the chordwise direction from leading to trailing edge with positive Y pointing outward from wing root for a right handed wing. All geometry indexing for the wing proceeds from the viscous wake trailing edge along the upper surface to the lower surface viscous wake trailing edge. Changes due to viscosity to the baseline configuration (jets-fuselage-wing without viscous effects) are allowed only on the wing surface. Thus, even though the presence of fuselage and jets is accounted for by the panel method calculation, the viscous-inviscid analysis procedure treats the wing as if it were isolated.

The geometric representation of the wing effective shape must interface with the Perturbation Analysis Method (Reference 12), which is used to compute the inviscid pressures. This method represents the effective shape as displacements in the Z direction from the baseline (Figure 18). These displacements are applied at the geometric defining stations, the panel corner points. The wing geometry is represented by panels with lines connecting corner points in the chordwise direction called defining span stations. However, all span stations cannot be independent since the number of prescribed pressures in the theoretical model must exceed the number of geometric perturbations for numerical stability (Reference 11). The even

numbered span stations on the wing are considered linearly dependent upon the two surrounding odd numbered span stations.

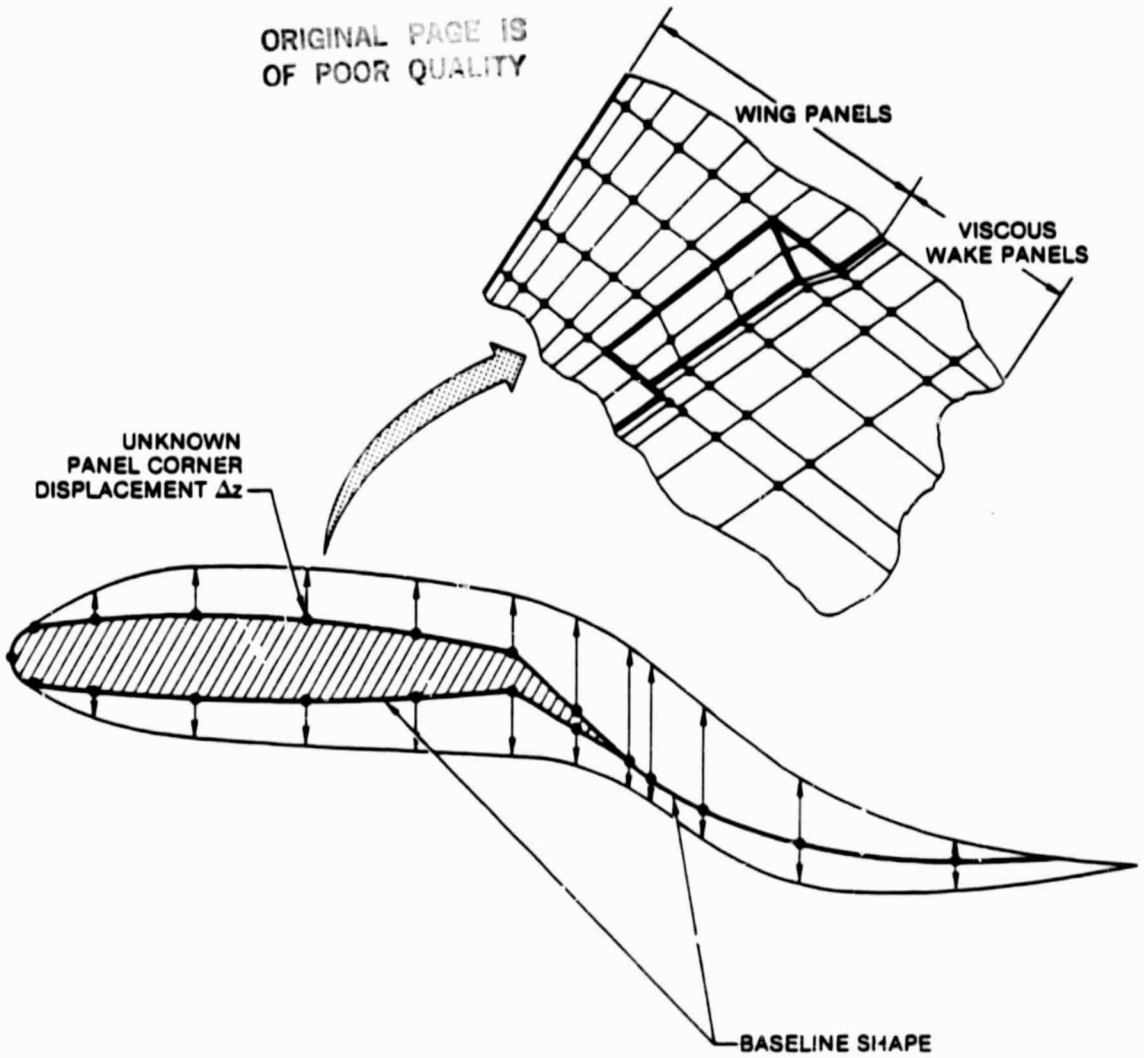

FIGURE 18. GEOMETRIC DESCRIPTION OF WING EFFECTIVE SHAPE

The viscous flow computations employ a body fitted non-orthogonal coordinate system (Figure 19), where X' is the surface distance from the upper surface viscous wake trailing edge, and

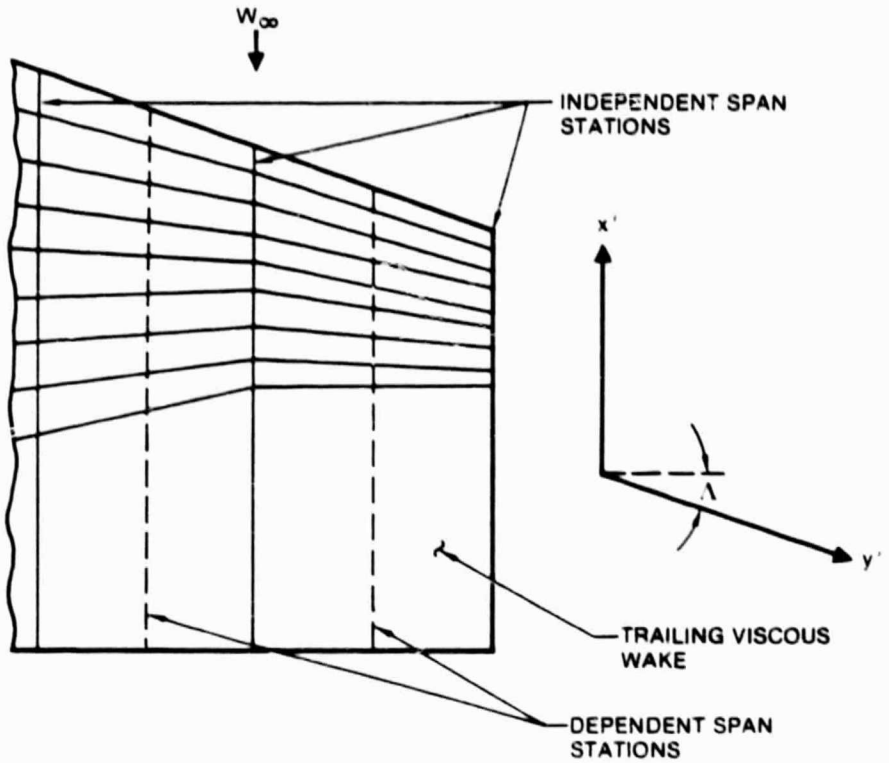

FIGURE 19. VISCOUS FLOW COORDINATE SYSTEM

Y' is parallel to the leading edge sweep. The wing surface is considered flat with Z' taken in the positive Z direction on the upper surface and in the negative Z direction on the lower surface. The surface distance to the panel cornerpoints, X', is given by:

$$X'_i = \sum_{j=j_1}^{i-1} \left[(X_{j+1} - X_j)^2 + (Z_{j+1} - Z_j)^2\right]^{\frac{1}{2}} \qquad (1)$$

where j_1 is the first panel cornerpoint on this span station. Z' is determined by first dividing each of the independent span stations into fourteen possible viscous regions (Figure 20) depending on the physics of the flow. Displacement of the wing effective shape is neglected in regions 6-9. The displacement of the remaining regions is represented by cubic polynomials based upon the values (X', Z', θ') at the region endpoints (Figure 21), where θ' is measured relative to baseline ($\theta' = \tan^{-1} \frac{dZ'}{dX'}$). Once the latest set of independent region endpoint conditions has been

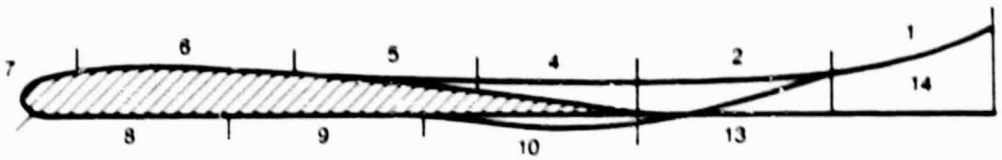

REGION NUMBER	VISCOUS REGION
1	AFT UPPER SURFACE VISCOUS TRAILING WAKE
2	FORE UPPER SURFACE VISCOUS TRAILING WAKE
3*	AFT UPPER SURFACE SEPARATED REGION
4**	FORE UPPER SURFACE SEPARATED REGION
5	AFT UPPER SURFACE TURBULENT FLOW
6	FORE UPPER SURFACE TURBULENT FLOW
7	UPPER SURFACE LAMINAR FLOW
8	LOWER SURFACE LAMINAR FLOW
9	FORE LOWER SURFACE TURBULENT FLOW
10	AFT LOWER SURFACE TURBULENT FLOW
11**	FORE LOWER SURFACE SEPARATED REGION
12*	AFT LOWER SURFACE SEPARATED REGION
13	FORE LOWER SURFACE VISCOUS TRAILING WAKE
14	AFT LOWER SURFACE VISCOUS TRAILING WAKE

*Exists only if separation is present ahead of flap hinge line
**Exists only if separation is present

FIGURE 20. VISCOUS REGIONS ALONG SPAN STATIONS

determined by the viscous-inviscid interaction procedure, the displacements at the panel corner points, ΔZ in Figure 18, are determined from:

$$\Delta Z_i = a_1 \xi_i^3 + a_2 \xi_i^2 + a_3 \xi_i + a_4 \tag{2}$$

where

$$\xi_i = \frac{X'_i - X'_A}{X'_B - X'_A} \tag{3}$$

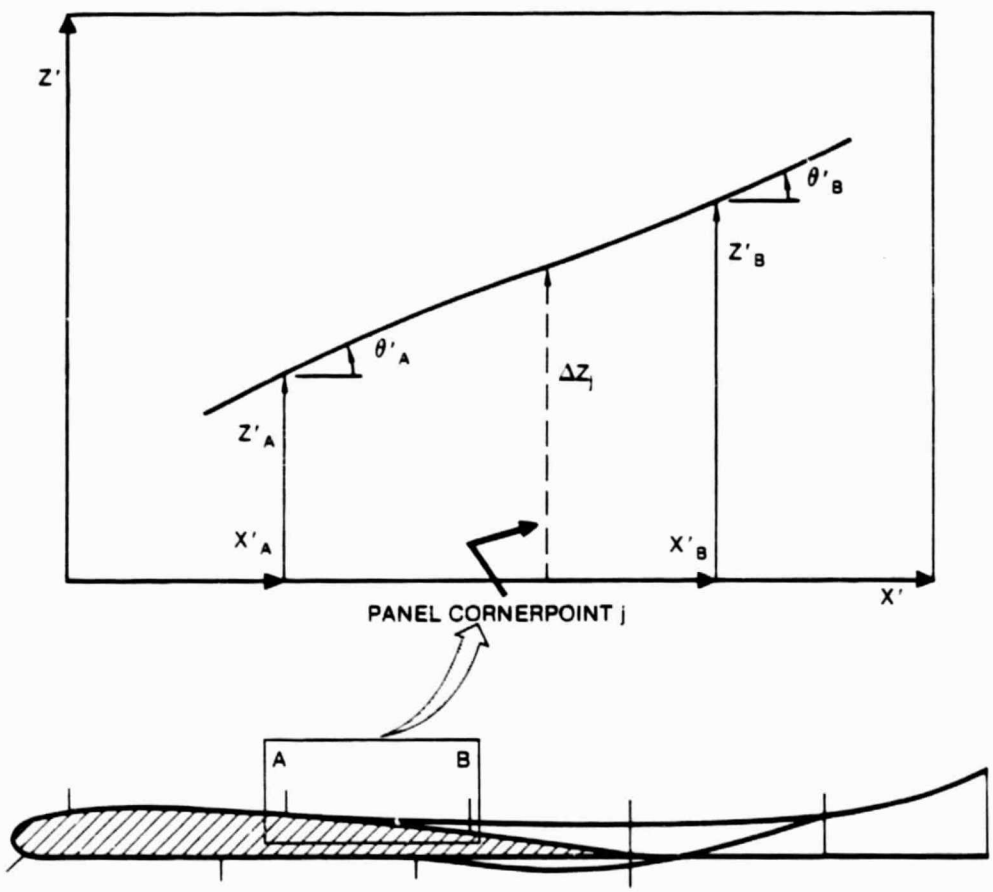

FIGURE 21. UNKNOWNS THAT SPECIFY A VISCOUS REGION

$$a_1, a_2, a_3, a_4 = \text{functions of } (X'_A, Z'_A, \theta'_A, X'_B, Z'_B, \theta'_B) \qquad (4)$$

The baseline configuration is allowed to have surface slope discontinuities at the flap hinge line, if flaps are present, and at the wing trailing edge. However, the wing effective shape must be continuous at all points except where the fore wake joins the aft wake (Figure 22) The baseline discontinuities are converted to a continuous displacement surface by requiring:

$$\theta'_A = \theta' + \theta'_D \qquad (5)$$

where

θ' = angle allowed to change during perturbation

θ'_D = discontinuous angle in baseline

Thus θ'_D accounts for the kink in the baseline shape.

At the fore wake trailing edge the effective shape is allowed to be discontinuous (See Figure 22). The downstream angle, θ_M, is required to be the bisector of the two upstream angles, θ'_{WU} and θ'_{WL}:

$$\theta'_{WM} = \frac{\theta'_{WU} + \theta'_{WL}}{2} \qquad (6)$$

The discontinuity is artifically introduced by requiring θ' and θ'_D in equation (5) to be (on the upper surface):

$$\theta' = \theta'_{WM} \tag{7}$$

$$\theta'_D = \theta'_{WU} - \theta'_{WM} \tag{8}$$

Similar equations are employed for the lower surface.

On the basis of numerical studies, it is reasonable to represent the length of the fore wake as a linear function of the thickness of the displacement surface at the wing trailing edge (See Figure 23). The curve shown in Figure 23 was generated from numerous computer solutions for different airfoils and Reynolds number by the Stalled Airfoil Analysis Program (Reference 7). This program solves for this length by requiring the velocity to be linear from the airfoil trailing edge value to approximately freestream at the wake trailing edge. However, in the present method, this procedure cannot be used due to the surface slope discontinuity in the effective shape at this point.

The turbulent boundary layer is divided into two regions, which are of equal length if flaps are not deflected or separation occurs upstream of the hinge line. Otherwise, the juncture between the two regions is fixed at the flap hinge line.

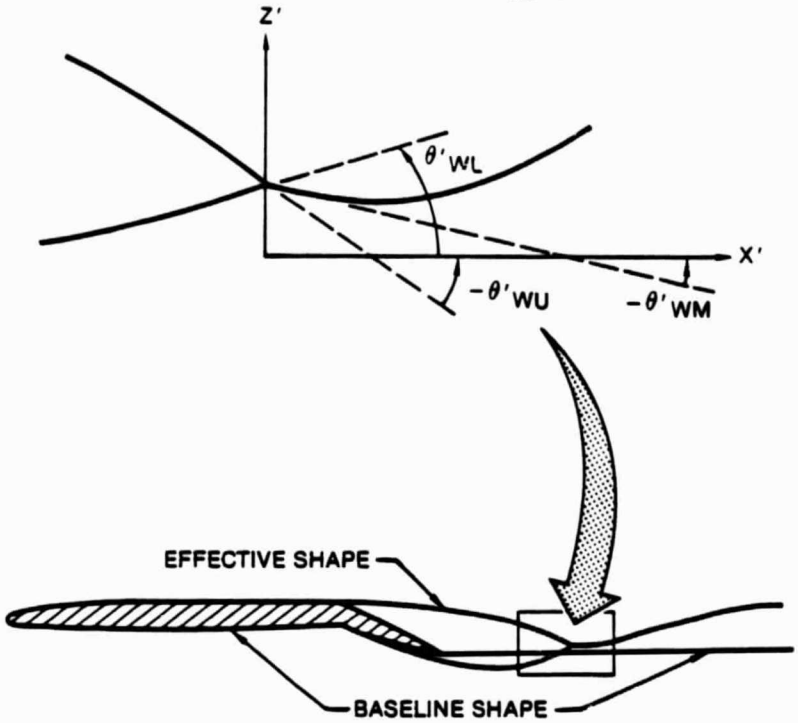

FIGURE 22. BASELINE SHAPE SHOWING SLOPE DISCONTINUITIES

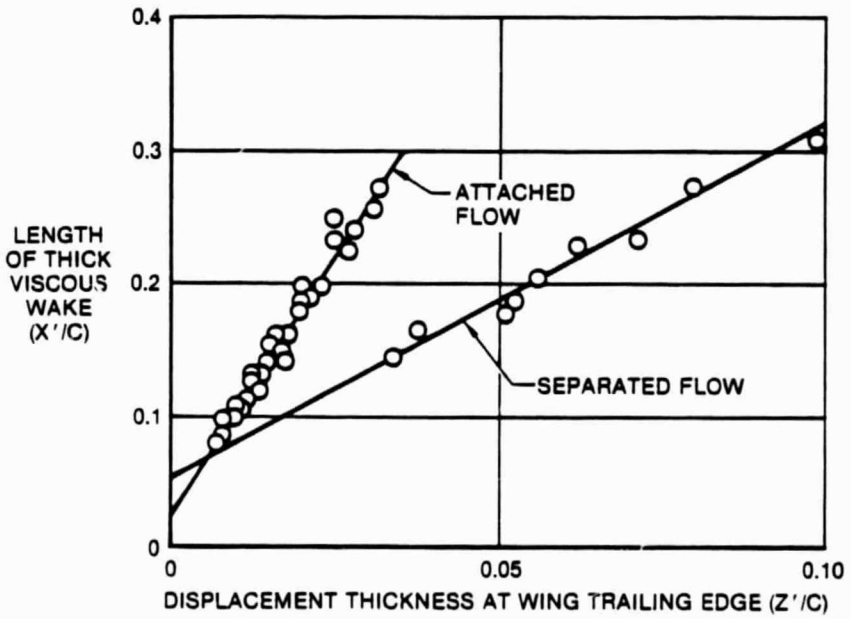

FIGURE 23. LENGTH OF THICK VISCOUS WAKE AS A FUNCTION OF DISPLACEMENT THICKNESS AT WING TRAILING EDGE (2-D)

The polynomial representation of the displacement surface in separated regions is made quartic in nature by the addition of another unknown displacement Z'_M, at the midpoint of the separation region. For these regions the displacement at panel cornerpoints is given by:

$$\Delta Z_i = \Delta Z_{C_i} + 16(Z'_M - Z'_{MC})(\xi_i^4 - 2\xi_i^3 + \xi_i^2) \qquad (9)$$

where ΔZ_{C_i} is given by equation (2) and Z_{M_C} is given by equation (2) for $\xi_i = .5$. Only one separation region is normally used on either the upper (P=4) or lower surface (P=11). However, when separation occurs ahead of the flap, both separation regions are employed with the endpoint between the two fixed at the hinge line.

Incorporation of the above assumptions and approximations and noting that the length of the trailing viscous wake is fixed, results in a relatively small set of independent unknowns, depicted in Figure 24 for the case of separation aft of the flap hinge line on the upper surface. The number of unknowns per span station can be as low as ten for no separation without laminar flow and can be as high as twenty for separation ahead of flap hinge line with laminar flow.

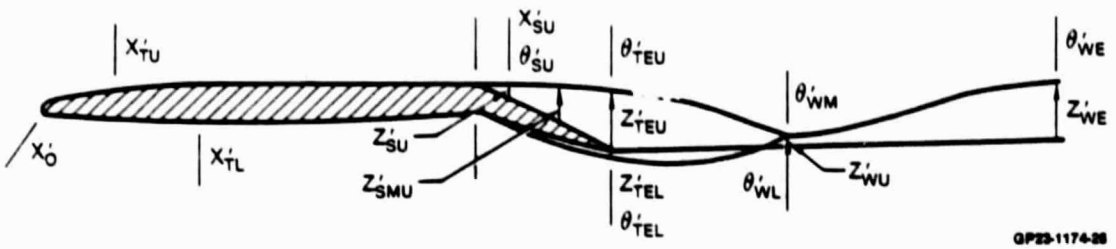

FIGURE 24. INDEPENDENT UNKNOWNS FOR A SPAN STATION WITH UPPER SURFACE SEPARATION AFT OF FLAP HINGE LINE

The set of independent unknowns across the wing can vary from one independent span station to another. The complete set of unknowns for the wing is stored in an array, called the "g-array":

$$\begin{bmatrix} g_1 \\ g_2 \\ \vdots \\ g_{N_{unk}} \end{bmatrix} \quad \begin{bmatrix} Z'_{WE} \\ \theta'_{WE} \\ \vdots \\ \theta'_{WL} \\ \vdots \\ \vdots \end{bmatrix} \quad \begin{matrix} \text{Independent} \\ \text{Span} = 1 \\ \\ 2 \\ \\ \vdots \\ \text{NSPANI} \end{matrix} \qquad (10)$$

The determination of the g-array that results in most closely satisfying the conditions of the theoretical model uniquely specifies the desired effective shape.

Calculation Procedure

The calculation procedure employed in the Stalled Wing Analysis Program is depicted in Figure 25. It is assumed that the geometric configuration to be analyzed has been previously analyzed by the MCAIR 3-D Subsonic Potential Flow Program and MCAIR 3-D Geometry Influence Coefficient Program. Thus, two matrices, corresponding to zero and ninety degree angles-of-attack, are available as input files. The elements of these matrices represent the first order rate of change of potential with respect to arbitrary changes in the ΔZ's on the independent span stations on the wing.

The user provides as input the freestream Reynolds number based on reference chord, velocity magnitude, and angle-of-attack range to be analyzed. In addition, the viscous geometry is chosen by specifying the number of calculation points and ξ_i distribution for each viscous region. An initial guess for the location of transition is chosen. The user also has options to fix transition at the input value, specify that the boundary layer flow on the wing be fully turbulent, or fix separation at an input location. From these input values, the g-array is initialized.

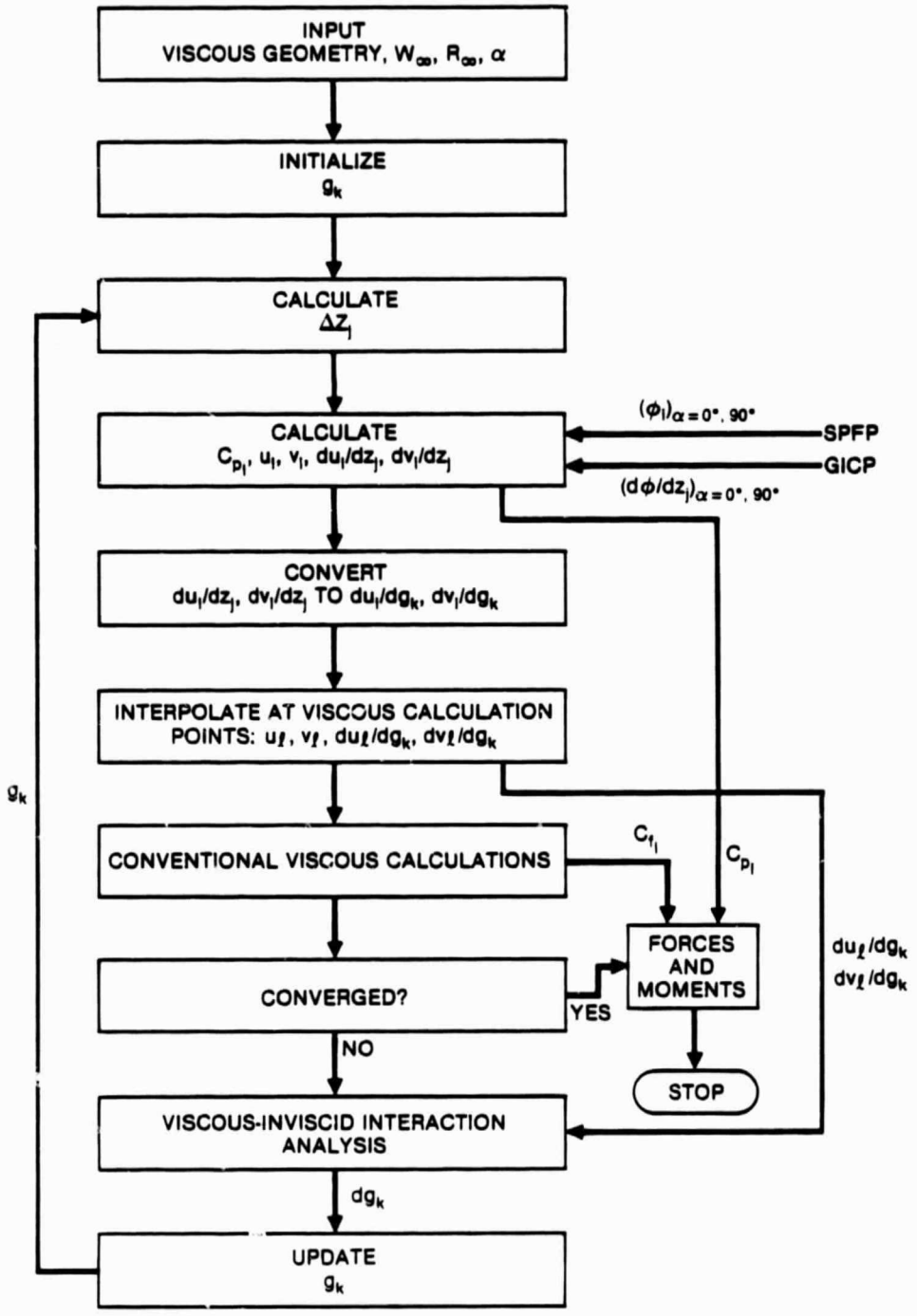

FIGURE 25. CALCULATION PROCEDURE OF STALLED WING ANALYSIS PROGRAM

Equations (2) - (9) are employed to determine the set of ΔZ_j from the g_k. The magnitude of the velocity at each panel center i is determined from Green's third identity (Reference 16) after the potential has been extrapolated from:

$$\phi_i = \cos\alpha\left(\phi_{0_i} + \sum_{j=1}^{NKS} \left(\frac{\partial \phi_i}{\partial Z_j}\right)_{\alpha=0^\circ} \Delta Z_j\right) + \sin\alpha\left(\phi_{90^\circ_i} + \sum_{j=1}^{NKS} \left(\frac{\partial \phi_i}{\partial Z_j}\right)_{\alpha=90^\circ} \Delta Z_j\right) \quad (11)$$

where ϕ_{0_i} and ϕ_{90_i} are the baseline potentials corresponding to $\alpha = 0^\circ$ and 90° from SPFP and NKS is the number of independent perturbations, ΔZ. The local velocity direction is determined from panel orientation, which allows the determination of the velocity components in the X, Y, and Z directions $(W_X, W_Y, W_Z)_i$. The tangential components of the inviscid velocity, U and V in the chordwise and spanwise direction are determined from:

$$U_i = \frac{W_{X_i} N_{Z_i} - W_{Z_i} N_{X_i}}{(N_{X_i}^2 + N_{Z_i}^2)^{1/2}} \quad (12)$$

$$V_i = W_{Y_i} \quad (13)$$

where $(N_X, N_Y, N_Z)_i$ are the components of the unit normal vector for the ith panel. This definition of U provides a negative value of U on the lower surface of the wing aft of the attachment line. Thus, the location of the attachment line, the boundary between the upper and lower surface laminar regions, can be determined from the point at which U is equal to zero along each span.

The pressure coefficient at the panel center, Cp_i, is calculated from Bernoulli's equation for steady flow:

$$Cp_i = 1 - \frac{U_i^2 + V_i^2}{W_\infty^2} \tag{14}$$

In addition, the rates of changes to U and V due to arbitrary changes in the Z_j can be calculated from equations (11) - (13) and the velocity direction equation. These coefficients are stored as $\frac{dU_i}{dZ_j}$ and $\frac{dV_i}{dZ_j}$. These matrices are converted to rates of change with respect to changes in the g-array by:

$$\frac{dU_i}{dg_k} = \frac{dU_i}{dZ_j} \cdot \frac{dZ_j}{dg_k} \tag{15}$$

$$\frac{dV_i}{dg_k} = \frac{dV_i}{dZ_j} \cdot \frac{dZ_j}{dg_k} \tag{16}$$

The $\frac{dZ_j}{dg_k}$ is determined by differentiation of equations (2), (3), (4), and (9).

The next step in the calculation procedure is to determine the conditions at the viscous calculation points, which are taken along the panel centers. The tangential velocity components, U_ℓ and V_ℓ, at these points are determined by cubic interpolation in the X' direction on U_i and V_i. Thus,

$$U_\ell = b_1 U_{i-1} + b_2 U_i + b_3 U_{i+1} + b_4 U_{i+2} + b_5 X'_{v\ell} \tag{17}$$

where

b_1, b_2, b_3, b_4, b_5 = coefficients based on interpolation routine

= functions of X'_{v_ℓ} (18)

and the location of the matching point X'_{v_ℓ}, is between U_i and U_{i+1}. From equations (17) and (18):

$$\frac{dU_\ell}{dg_k} = b_1 \frac{dU_{i-1}}{dg_k} + b_2 \frac{dU_i}{dg_k} + b_3 \frac{dU_{i+1}}{dg_k} + b_4 \frac{dU_{i+2}}{dg_k} + \left(b_5 + \sum_{k=1}^{5} \frac{\partial b_k}{\partial X'_{v_\ell}}\right) \frac{dX'_{v_\ell}}{dg_k} \tag{19}$$

Similar calculations are performed for V.

The values of X'_v and Z'_v are determined from the y-array:

$$X'_{v_\ell} = \frac{\Delta y(2)}{\Delta y(1) + y(2)} \cdot \xi_\ell \, (X'_{B_L} - X'_{A_L}) + \frac{\Delta y(1)}{\Delta y(1) + y(2)} \cdot \xi_\ell \cdot (X'_{B_R} - X'_{A_R}) \tag{20}$$

$$Z'_{v_\ell} = \frac{\Delta y(2)}{\Delta y(1) + \Delta y(2)} \cdot Z'_L + \frac{\Delta y(1)}{\Delta y(1) + \Delta y(2)} \cdot Z'_R \tag{21}$$

where $\Delta y(1)$, and $\Delta y(2)$ are defined in Figure 26, L and R refer to left and right independent span stations surrounding the panel centers being calculated, ξ_ℓ is the input value of ξ:

$$\xi_\ell = \frac{X'_\ell - X'_A}{X'_B - X'_A} \tag{22}$$

A and B refer to region endpoint conditions. Z'_L and Z'_R are determined from equations (2), (3), (4) and (9). $\frac{dX'_{v_\ell}}{dg_k}$ and $\frac{dZ'_{v_\ell}}{dg_k}$ are determined by differentiating equations (20) and (21).

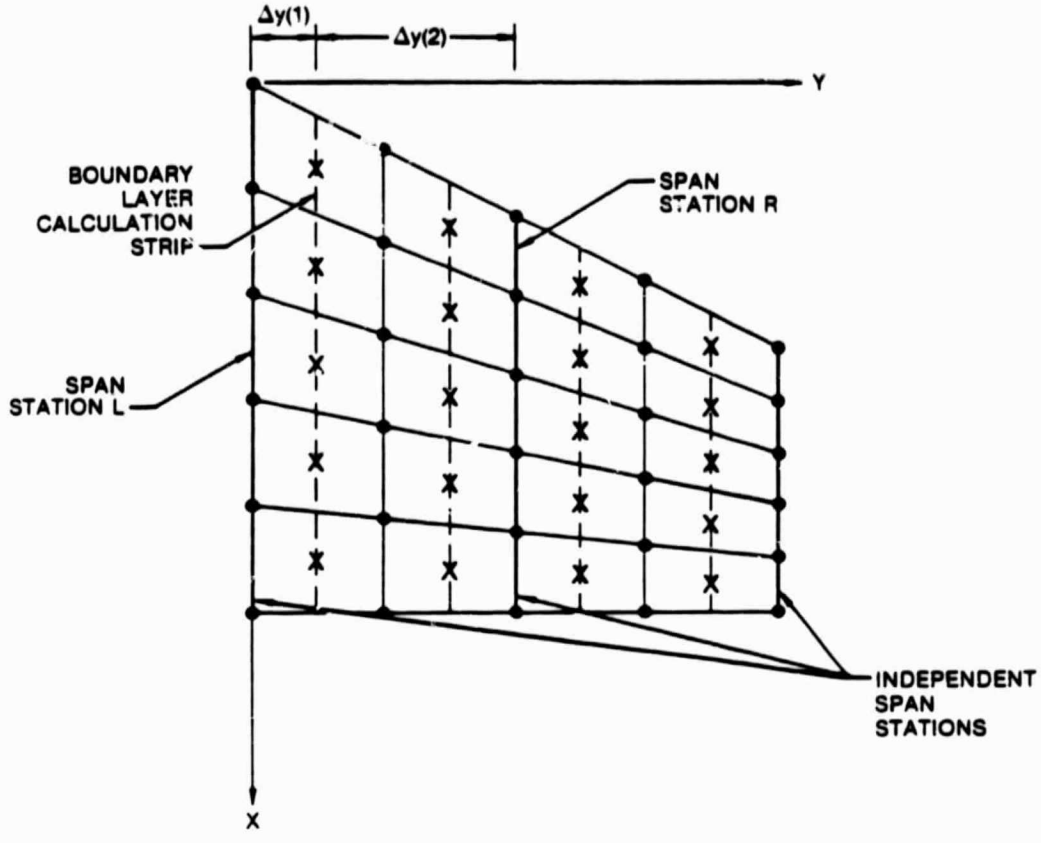

FIGURE 26. SCHEMATIC OF BOUNDARY LAYER CALCULATION POINTS

Once the inviscid conditions are established at the boundary layer calculation points, the viscous parameters can be determined. In addition to the inviscid parameters previously discussed, the boundary layer calculation routines require gradients in the X and Y directions of the velocity components U and V: U_x, U_y, V_x, V_y. The X direction gradients are established by differentiating equation (17) for U_x and the analog for V_x. The

Y direction gradients are calculated from differentiation of a quadratic curve fit in the Y direction. These terms are also differentiated with respect to g to establish the perturbation matrices.

The boundary layer calculation methods are based on the hypothesis that the viscous flow can be divided into components in the mainflow and crossflow direction with the components behaving much like two-dimensional flow. A sketch of the boundary layer coordinate system is depicted in Figure 27. The angle between the projection of the external streamline onto the surface and the X' axis, denoted γ, is the direction of the mainflow. The crossflow direction is taken perpendicular to this direction in the positive Y' direction. The angle between the mainflow direction and the limiting wall streamline, the direction of surface shear, is denoted β. This angle is a measure of the magnitude of the skewing in the Z' direction of the flow with the boundary layer and is a measure of how three-dimensional the viscous flow is. All of the viscous calculation methods are used to compute the growth of the boundary layer, which is characterized by four parameters. These are the momentum thickness in the mainflow direction, T_E, the boundary layer shape factor in the mainflow direction, H, the limiting wall streamline angle, β, and the viscous displacement thickness, δ^*.

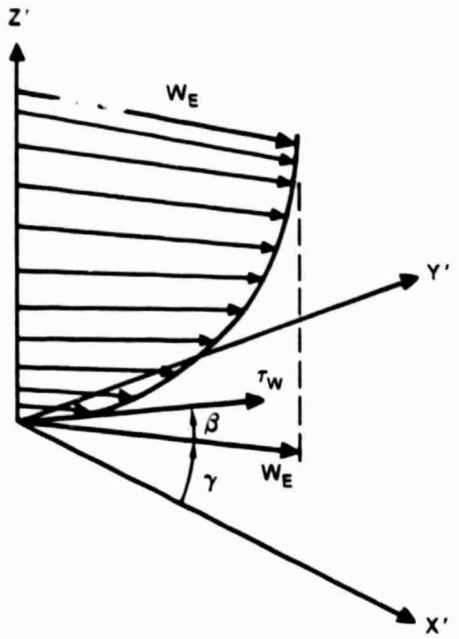

FIGURE 27. GEOMETRY WITHIN BOUNDARY LAYER

Along the attachment line the laminar flow equations at point ℓ are:

$$T_{E_\ell} = \frac{.407\ C_\ell^{*1/2}}{R_\infty\ U_{E_\ell}} \tag{23}$$

$$C_\ell^* = \frac{R_\infty\ U_{E_\ell}^{\ 2}}{(U_{x_\ell} + V_{y_\ell} - U_{E_{y\ell}})} \tag{24}$$

$$U_{E_\ell} = (U_\ell^{\ 2} + V_\ell^{\ 2})^{1/2} \tag{25}$$

$$\beta_\ell = 0 \tag{26}$$

$$H_\ell = 2.54 \tag{27}$$

$$\delta_\ell^* = 0. \tag{28}$$

The shape factor is chosen arbitrarily. The derivative of these equations with respect to g_k must be established. As an example, consider equation (23):

$$\frac{\partial T_{E_\ell}}{\partial g_k} = \frac{T_{E_\ell}}{2C^*_\ell} \frac{\partial C^*_\ell}{\partial g_k} - \frac{T_{E_\ell}}{U_{E_\ell}} \frac{\partial U_{E_\ell}}{\partial g_k} \tag{29}$$

By differentiating equations (24) and (25) and noting that U_x and V_y are determined from the surrounding U_i and V_i, X', and Y', equation (29) can be expressed as:

$$\frac{\partial T_{E_\ell}}{\partial g_k} = C_1 \frac{\partial U_\ell}{\partial g_k} + C_2 \frac{\partial V_\ell}{\partial g_k} + C_3 \frac{\partial X'_\ell}{\partial g_k} \tag{30}$$

Substituting expressions for the derivatives appearing in equation (30) results in $\frac{\partial T_{E_\ell}}{\partial g_k}$ becoming a vector with each element representing the rate of change of T_E with respect to change in the kth element of the g array. Differentiating equations (26)-(28) results in:

$$\frac{\partial \beta_\ell}{\partial g_k} = \frac{\partial H}{\partial g_k} = \frac{\partial \delta^*_\ell}{\partial g_k} = 0 \tag{31}$$

Each of the equations in the viscous flow computation procedure is differentiated. Most are successive application of the chain rule, illustrated above. Therefore, the mathematical

expansions for the remaining equations will not be presented, for clarity, unless the procedure employed differs substantially from the above example.

Transition along the attachment line is specified by the Reynolds number based on momentum thickness, R_T, being greater than 100. Turbulent attachment line flow development is calculated from a linear curve fit to the $M_\infty = 0$ solution of Smith's method (Reference 22):

$$T_{E_\ell} = \frac{.0016925\ C_\ell^* + 83.75}{R_\infty\ U_{E_\ell}} \tag{32}$$

$$\delta_\ell = 0 \tag{33}$$

$$H_\ell = 1.45 \tag{34}$$

$$\delta_\ell^* = 0. \tag{35}$$

The value for the shape factor, H_ℓ, is chosen arbitrarily.

The attachment line values of the viscous parameters are used as starting conditions for the remainder of the boundary layer computations. The viscous geometry on the wing is depicted in Figure 28 for the example case of fully attached flow, attachment line at the leading edge, and transition to turbulence along the attachment line halfway across the span. Each of the same type of viscous regions across the span is divided into a user supplied number of boundary layer calculation points. Each

of these points correspond to the intersection of lines along the panel centers and lines of constant ξ. The local nonorthogonal coordinate system is based on lines of constant y and constant with the angle between the two denoted λ.

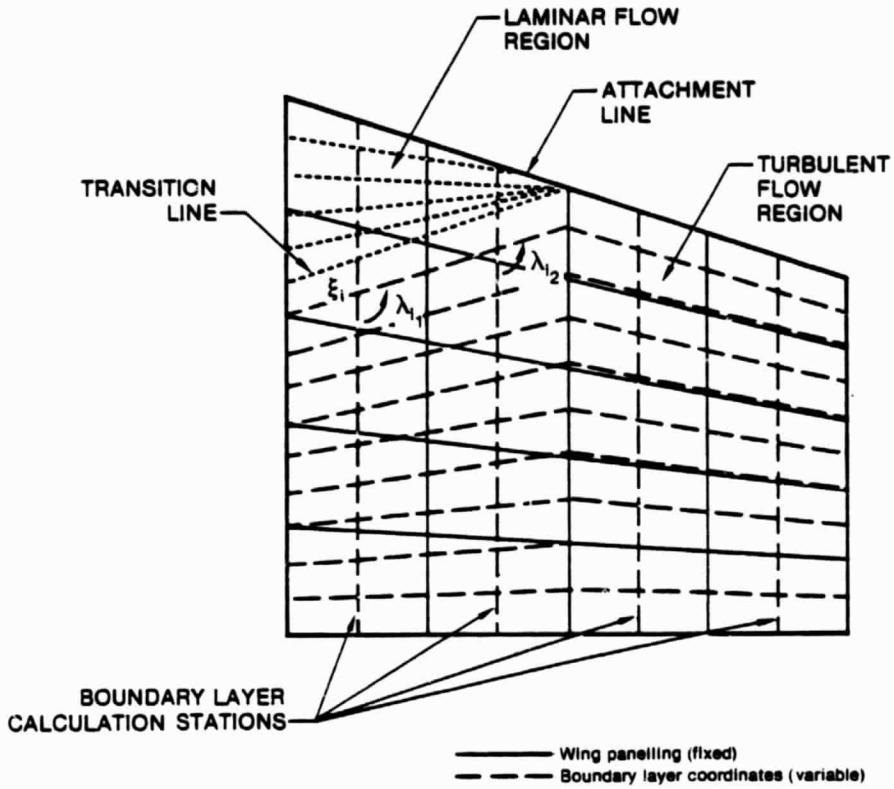

FIGURE 28. VISCOUS REGION GEOMETRY FOR A SWEPT, TAPERED WING

The generalized nonorthogonal coordinate system introduces metric coefficients into the viscous equations. These coefficients (h_1, h_2) represent the coordinate stretching factors, where an element of length ds on the body surface is given by:

$$ds^2 = h_1^2 dx'^2 + h_2^2 dy'^2 + h_1 h_2 \cos \lambda \, dx' dy'$$

h_1 and h_2 are dependent on X' and Y' and are described in Appendix I.

The flow in the laminar or turbulent regions is calculated by integrating the equations of motion in the X' direction (attachment line to trailing edge). The slopes of the T_E, β, and H terms are calculated at the latest points at which these terms are known from equations of the form:

$$\sum_{j=1}^{3} C_{kj} \left(\frac{dv}{dx'}\right)_j = RHS_k \qquad (37)$$

C_{kj} = Coefficients based on the values of T_E, β, H, U, V h_1, h_2, X', and Y'.

$$\left(\frac{dv}{dx'}\right)_j = \frac{dT_E}{dx'}, \frac{d\beta}{dx'}, \frac{dH}{dx'} \quad j = 1,2,3$$

RHS_k = Right hand sides, based on values of T_E, β, H, U, V, h_1, h_2, X', and Y'.

Both the laminar and turbulent flow equations are of the form of equation (37); however, the laminar flow equations, being a small crossflow method, reduce to a 2x2 system of linear equations. The solution to equation (37) is established by simple linear algebra:

$$\left(\frac{dv}{dX'}\right)_j = \sum_{k=1}^{3} C_{jk}^{-1} RHS_k \qquad (38)$$

Trapezoidal rule integration is performed resulting in the projected value of T_E, β, and H at point $\ell+1$:

$$v_{\ell+1,j} = v_{\ell,j} + \left(\frac{dv}{dx'}\right)_{\ell,j} \Delta X'_{\ell} \tag{39}$$

The displacement thickness does not appear explicitly in the equations of motion in three-dimensional boundary layers. Rather, the displacement thickness slope is calculated from the continuity equation and is of the form:

$$\frac{d\delta^*}{dX'} = RHS_4 \tag{40}$$

where

RHS_4 = Right hand side, based on values of $\frac{dT_E}{dX'}$, $\frac{d\beta}{dX'}$, $\frac{dH}{dX'}$, δ^*, U, V, h_1, h_2, X', and Y'.

This equation is also integrated in the X' direction

$$\delta^*_{\ell+1} = \delta^*_{\ell} + \left(\frac{d\delta^*}{dX'}\right)_{\ell} \Delta X'_{\ell} \tag{41}$$

This equation is only applied in regions where the displacement thickness is modelled.

Equations (37)-(41) must be differentiated with respect to g_k. Working backwards:

$$\frac{\partial \delta^*_{\ell+1}}{\partial g_k} = \frac{\partial \delta^*_{\ell}}{\partial g_k} + \left(\frac{d\delta^*}{\partial X'_{\ell}}\right) \frac{\partial (\Delta X'_{\ell})}{\partial g_k} + X' \frac{\partial \left(\frac{d\delta^*}{\partial X'}\right)_{\ell}}{\partial g_k} \qquad (42)$$

$\frac{\partial \delta^*_{\ell}}{\partial g_k}$ is known from the previous upstream point calculation.

$\frac{\partial (\Delta X'_{\ell})}{\partial g_k}$ is available from differentiating equation (20).

$\frac{\partial}{\partial g_k}\left(\frac{\partial \delta^*}{\partial X'}\right)_{\ell}$ is determined from equation (40):

$$\frac{\partial}{\partial g_k}\left(\frac{d\delta^*}{dX'}\right)_{\ell} = \frac{\partial}{\partial g_k}(RHS4)_{\ell} \qquad (43)$$

$$(RHS4)_{\ell} = f\left(\frac{dT_E}{dX'}, \frac{d_\beta}{dX'}, \frac{dH}{X'}, \delta^*, U, V, h_1, h_2, X', Y'\right)_{\ell} \qquad (44)$$

$$\frac{\partial (RHS_4)_{\ell}}{\partial g_k} = \frac{\partial f}{\partial \left(\frac{dT_E}{dX'}\right)} \frac{\partial \left(\frac{dT_E}{dX'}\right)}{\partial g_k} + \frac{\partial f}{\partial \left(\frac{d\beta}{\partial X'}\right)} \frac{\partial \left(\frac{d\beta}{\partial X'}\right)}{\partial g_k} + \frac{\partial f}{\partial \left(\frac{dH}{\partial X'}\right)} \frac{\partial \left(\frac{dH}{\partial X'}\right)}{\partial g_k}$$

$$+ \frac{\partial f}{\partial \delta^*} \frac{\partial \delta^*}{\partial g_k} + \frac{\partial f}{\partial U} \frac{\partial U}{\partial g_k} + \frac{\partial f}{\partial V} \frac{\partial V}{\partial g_k} + \frac{\partial f}{\partial h_1} \frac{\partial h_1}{\partial g_k}$$

$$+ \frac{\partial f}{\partial h_2} \frac{\partial h_2}{\partial g_k} + \frac{\partial f}{\partial X'} \frac{\partial X'}{\partial g_k} + \frac{\partial f}{\partial Y'} \frac{\partial Y'}{\partial g_k} \qquad (45)$$

The $\frac{\partial \delta^*}{\partial g_k}$ is available from the previous upstream point calculation. $\frac{\partial u}{\partial g_k}$ and $\frac{\partial v}{\partial g_k}$ are available from the inviscid differentiations. $\frac{\partial h_1}{\partial g_k}$, $\frac{\partial h_2}{\partial g_k}$, and $\frac{\partial Y'}{\partial g_k}$ are determined from X', and $\frac{\partial X'}{\partial g_k}$ is available from differentiating equation (20). The derivatives of the slope of T_E, β, and H are determined by differentiating equation (38):

$$\frac{\partial}{\partial g_k} \sum_{j=1}^{3} C_{ij}\left(\frac{dv}{\partial X'}\right)_j = \frac{\partial}{\partial g_k} RHS_i \qquad (46)$$

$$\sum_{j=1}^{3} \left(C_{ij} \frac{\partial}{\partial g_k}\left(\frac{\partial v}{\partial X'}\right)_j + \frac{\partial C_{ij}}{\partial g_k} \cdot \left(\frac{dv}{\partial X'}\right)_j\right) = \frac{\partial RHS_i}{\partial g_k} \qquad (47)$$

$$\frac{\partial}{\partial g_k}\left(\frac{dv}{dX'}\right)_i = \sum_{i=1}^{3} C_{ji}^{-1}\left(\frac{\partial RHS_i}{\partial g_k} - \sum_{j=1}^{3} \frac{\partial C_{ij}}{\partial g_k} \left(\frac{dv}{dX'}\right)_j\right) \qquad (48)$$

The C_{ji}^{-1} and $\left(\frac{dv}{dX'}\right)_j$ terms are known from equation (38). The derivatives of RHS_i and C_{ij} are determined much the same as accomplished for RHS_4 in equation (45). Equation (39) is also differentiated to establish expressions for $\frac{\partial T_{E_\ell}}{\partial g_k}$, $\frac{\partial B_\ell}{\partial g_k}$, and $\frac{\partial H_\ell}{\partial g_k}$.

Each of the terms in the mathematical expressions are stored as matrices, A, B, C, and D, defined by the following expressions:

$$dU_\ell = \sum_{k=1}^{N_{unk}} A_{\ell k}\, dg_k \qquad (49)$$

$$dV_\ell = \sum_{k=1}^{N_{unk}} B_{\ell k}\, dg_k \qquad (50)$$

$$dH_\ell = \sum_{k=1}^{N_{unk}} C_{\ell k}\, dg_k \qquad (51)$$

$$d\delta^*_\ell = \sum_{k=1}^{N_{unk}} D_{\ell k}\, dg_k \qquad (52)$$

These matrices are retained for use in the viscous-inviscid interaction procedure.

The skin friction at each boundary layer calculation point C_{f_ℓ}, is calculated from expressions found in the selected

methods. The wall shear stress acts on the surface in the direction of the limiting wall streamline. Thus, the skin friction force acting in the chordwise direction tangential to the panel surface is:

$$C_{f_{X'}} = C_{f_\ell} \cos(\gamma + \beta) \tag{53}$$

These values are converted to mean values on each surface panel by length weighting.

The forces and moments on the aircraft surface are determined by integrating the pressure coefficient, C_{p_i}, over the aircraft surface and the skin friction over the surface of the wing. A test for convergence based on a .01 change in the wing lift coefficient is made.

The viscous-inviscid interaction is explicitly modelled by finding the set of dg_k that most nearly satisfies to first order the conditions of the theoretical model. The theoretical model can be mathematically stated as follows:

Aft Attached Flow: $$\delta^*_\ell = Z' \tag{54}$$

Separated Flow: $$C_{p_\ell} = C_{p_{sep}} \tag{55}$$

Wing/Trailing Edge: $$C_{p_{upr}} = C_{p_{lwr}} \tag{56}$$

Fore Wake: $$C_p = C_{p_{TE}} + \frac{S_\ell}{S_{TOT}} (C_{p_{WTE}} - C_{p_{TE}}) \tag{57}$$

Aft Wake: $$C_{p_{upr_\ell}} = C_{p_{lwr_\ell}} \tag{58}$$

where S is surface distance from wing trailing edge, S_{TOT} is surface distance from wing trailing edge to fore wake trailing edge, $C_{P_{TE}}$ is average value of C_p at wing trailing edge at each span, $C_{P_{WTE}}$ is value of desired C_p at fore wake trailing edge at each span (input by user), and $C_{P_{sep}}$ is the C_p at each of the separation points.

A first order mathematical expansion of equations (54-58) results in:

$$\delta^*_\ell + d\delta^*_\ell = Z'_\ell + dZ'_\ell \tag{59}$$

$$C_{P_\ell} + dC_{P_\ell} = C_{P_{sep}} + dC_{P_{sep}} \tag{60}$$

$$C_{P_{upr}} + dC_{P_{upr}} = C_{P_{lwr}} + dC_{P_{lwr}} \tag{61}$$

$$C_{P_\ell} + dC_{P_\ell} = \left(1 - \frac{S_\ell}{S_{TOT}}\right) dC_{P_{TE}} \tag{62}$$

$$C_{P_{upr_\ell}} + dC_{P_{upr_\ell}} = C_{P_{lwr_\ell}} + dC_{P_{lwr_\ell}} \tag{63}$$

Noting that:

$$\frac{\partial C_p}{\partial g_k} = \frac{-2}{W_\infty^2}\left(U \frac{\partial U}{\partial g_k} + V \frac{\partial V}{\partial g_k}\right) \tag{64}$$

and substituting equations (49)-(52) for the aerodynamic perturbations, and derivatives of equation (21) for dZ' , equations (59)-(63) can each be written in the form:

$$\epsilon_i - \sum_{k=1}^{N_{UNK}} E_{ik}\, dg_k = 0 \tag{65}$$

where ε_i is the difference in desired conditions, e.g., $\varepsilon_\ell = Z'_\ell - \delta^*_\ell$, and the remainder of the equation is just the first order change in ε, e.g.,

$$d\,\varepsilon_\ell = dZ'_\ell - d\delta^*_\ell = -\sum_{k=1}^{N_{UNK}} E_{\ell k}\, dg_k \qquad (66)$$

The appropriate equation for each viscous region type is applied at each viscous matching point. The solution to this set of linear equations would represent the changes in the displacement and slope at the region endpoints to satisfy the conditions of the theoretical model. However, additional equations are necessary to establish the X' location of each region endpoint. These equations, called region endpoint constraints, are necessary at each region endpoint that represents an independent unknown in the g array. These are the attachment line, transition location, and separation location.

The desired condition at the attachment line is that the tangential velocity on the chordwise direction, U, be zero. Thus, the perturbation form of the equation is:

$$U_{ATTCH} + dU_{ATTCH} = 0. \qquad (67)$$

The transition constraint equation for eitner the upper or lower surface is based on four possibilities: fixed by user,

mainflow transition, crossflow transition, or laminar separation. If the user elects to fix transition at a constant local chord fraction, the fraction is automatically converted to an X' location, X'_{TR}. If X'_i is the value of X' at the transition location initially, the perturbation form of the constraint equation is:

$$X'_i + dX'_i = X'_{TR} \tag{68}$$

Mainflow transition is indicated by the Reynolds number based on momentum thickness, R_T, being equal to a curve fit value of critical momentum thickness Reynolds number, R_{TT}. R_{TT} is a function of Reynolds number based on surface distance R_X and the constraint equation is of the form:

$$R_T + dR_T = R_{TT} + dR_{TT} \tag{69}$$

Crossflow instability is indicated by the crossflow Reynolds number based on boundary layer thickness, R_{n_s}, exceeding a critical value. Since a change in the crossflow transition point would require a change on the geometry in the y direction, this equation cannot be applied explicitly. Rather, the most upstream location of calculated crossflow transition, if indicated, for each span strip replaces X'_{TR} in equation (68). Laminar separation is indicated by the mainflow laminar shape factor, H, exceeding 4.0. The constant equation representing the condition is:

$$H + dH = 4.0 \tag{70}$$

The turbulent separation point is based on the mainflow turbulent shape factor, H, exceeding 2.0. Thus;

$$H + dH = 2.0 \tag{71}$$

Equations (68)-(71) are also converted to the form of equation (65) by substitution of aerodynamic perturbations and geometric perturbations. The number of equations exceeds the number of unknowns. Thus, a method of least square errors is applied to obtain the solution g array.

The solution procedure is to minimize an error function F, where:

$$F = \underset{Z', \theta' \text{ Equations}}{\Sigma WT_i(\varepsilon_i - \Sigma_j E_{ij} dg_j)^2} + \underset{X' \text{ Contraints}}{\Sigma\ WT_k(\varepsilon_k - \Sigma_j E_{kj} dg_j)} \tag{72}$$

The first term in equation (72) represents the appropriate equation from equations (59) - (63). The weighting of each equation, WT_i, is based on surface distance and user supplied region weighting, WT_p:

$$WT_i = (X'_{i+1} - X'_i)\ WT_p \tag{73}$$

The region weight is used to force the boundary layer type equations, equation (59), to be as important as the inviscid

equations, equations (60)-(63). Normally, a 10,000 to 1 ratio is satisfactory.

The second term in equation (72) represents the region end-point constraint equations, equations (68)-(71). The weight WT_k is calculated automatically in the method and is used to keep all of these equations more important than equations in the first term.

The method for solving equation (72) is to differentiate F with respect to each unknown, dg, and set the resulting terms to zero. This converts F to a system of N_{UNK} linear equations, which is solved by standard linear algebra.

This procedure results in a calculated vector dg_k. The g array may then be updated:

$$g'_k = g_k + dg_k \tag{74}$$

The calculation procedure is then returned to the calculation of the ΔZ's.

This iterative procedure is continued until convergence is obtained. This procedure is employed typically over a range of angles-of-attack in two degree increments. The last converged solution geometry provides the initial guess for the succeeding

angle-of-attack. Convergence is achieved normally in two to three iterations.

EXAMPLE CALCULATIONS

To be able to assess the accuracy of the jet-airframe-wing viscous effects predictions, several wing alone calculations were performed prior to analyzing the YAV-8B powered model. These example computations were supported by the MCAIR 1982 Independent Research and Development Program. However, these solutions are presented here for completeness. The wing alone geometric parameters chosen for analysis are shown in Table I along with the YAV-8B supercritical wing. Each of these solutions is discussed.

TABLE I. WING GEOMETRIES ANALYZED

WING SECTION	ASPECT RATIO	LEADING EDGE SWEEP ANGLE (deg)	TAPER RATIO	TWIST (deg)
NACA 4412	6.0	0	0	0
NACA 0012	5.5	20.00	0	0
NACA 64_1 – 212	6.0	37.25	0.5	0
YAV-8B SUPERCRITICAL (0.11 t/c ROOT, 0.07 t/c TIP)	4.0	36.00	0.3	– 8.0

NACA 4412 Rectangular Wing

The first wing alone geometry analyzed was a rectangular planform, NACA 4412 section, aspect ratio 6 wing. Since

experimental force and moment data were available for this wing at midspan, it was possible to assess the accuracy of the method without having to deal with strong three dimensional boundary layer effects. The predicted force and moment at midspan are compared with experiment (Reference 27) in Figure 29. The predictions agree well with experiment. Furthermore, this section geometry was analyzed by the Stalled Airfoil Analysis Program (Reference 7) with results depicted in Figure 30. Comparison of Figure 29 and 30 show that the present method exhibits the same trends as the two dimensional method. This result provides confidence in using the polynomial curve fits to represent the boundary layer thickness and the Perturbation Analysis Method to calculate the inviscid parameters, since the Stalled Airfoil Analysis Program does not use either of these approximations.

NACA 0012 Swept Wing

The next case analyzed was a 20° swept, NACA 0012 section, aspect ratio 5.5 wing on a wall. The predicted forces and moments are depicted in Figure 31. While experimental data in the form of pressure distributions along lines normal to the leading edge are available (Reference 28), overall force and moment data are not available. The only force data found in this data set was the normal force, C_N, on an unswept, NACA 0012 section, aspect ratio 6 wing. Thus, this wing geometry was analyzed and the predicted normal force is compared with experiment in Figure 32. Also shown is the predicted normal force for the swept wing

case, which follows reasonable trends when compared to the unswept data.

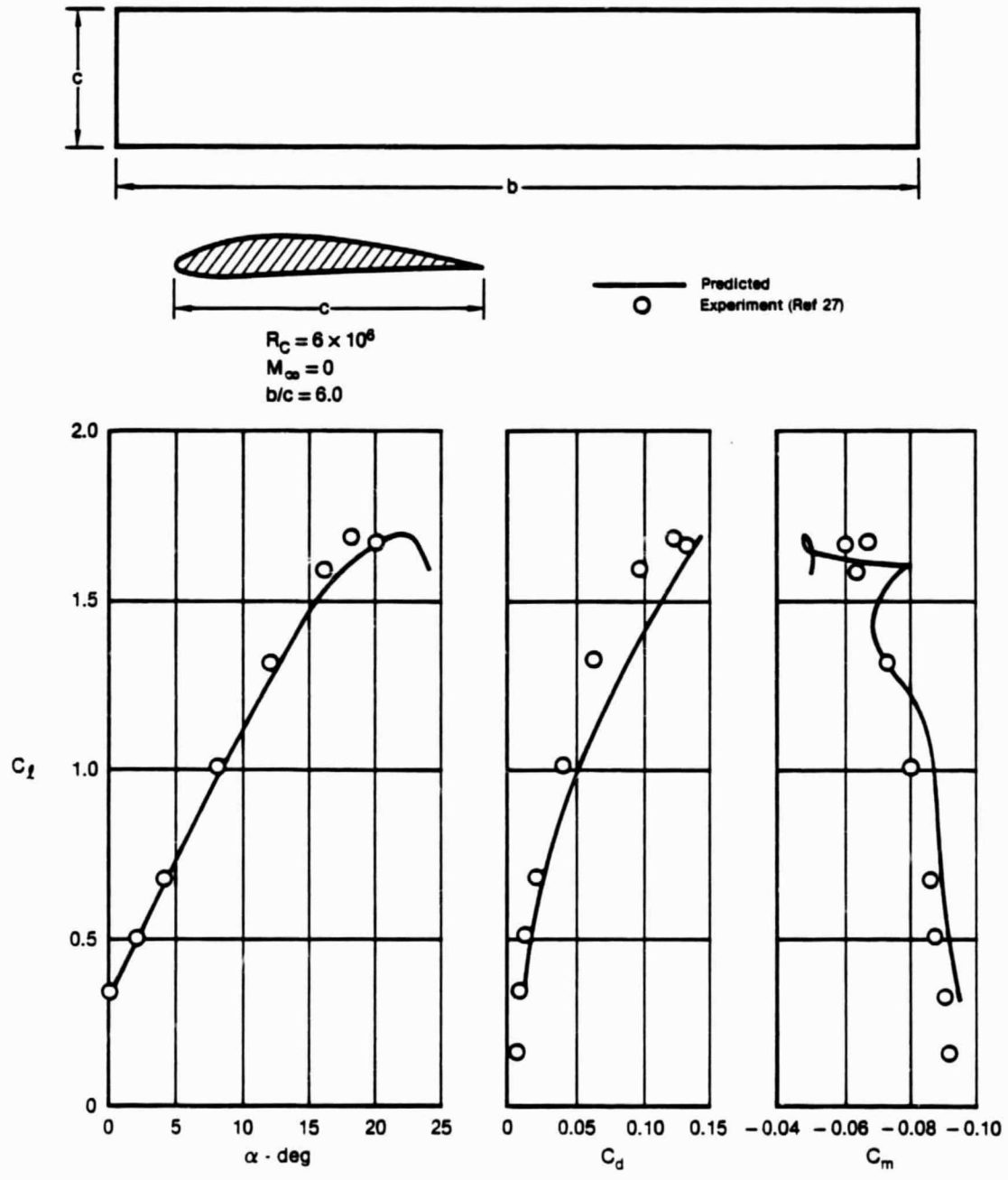

FIGURE 29. FORCE AND MOMENT PREDICTION AT MIDSPAN OF A NACA 4412, ASPECT RATIO 6, RECTANGULAR WING

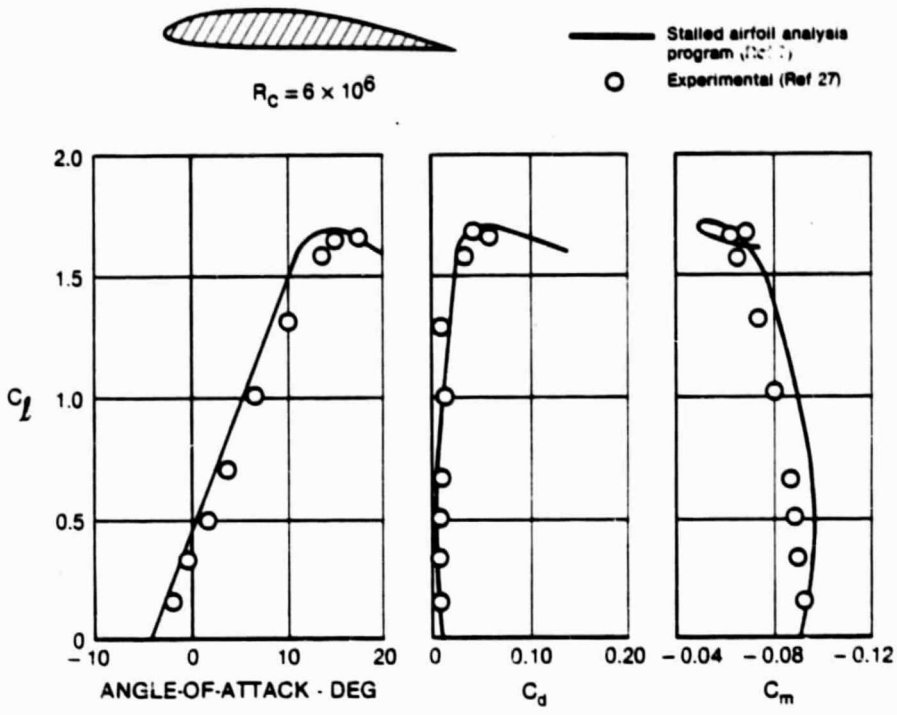

FIGURE 30. FORCE AND MOMENT PREDICTIONS
NACA 4412 Airfoil

While analyzing the swept wing case, it was discovered that the laminar boundary layer calculations tended to become numerically unstable near the suction peak at high angles-of-attack ($> 15°$). It is believed that the primary cause for the instabilities was that the transition constraint equations did not move the transition location far enough forward to preclude the presence of very strong adverse pressure gradients within the laminar viscous regions. Successful analysis was accomplished by considering the flow to be fully turbulent from the attachment

line and fixing the beginning of the upper surface turbulent region at the leading edge. This procedure was also used for the remaining cases.

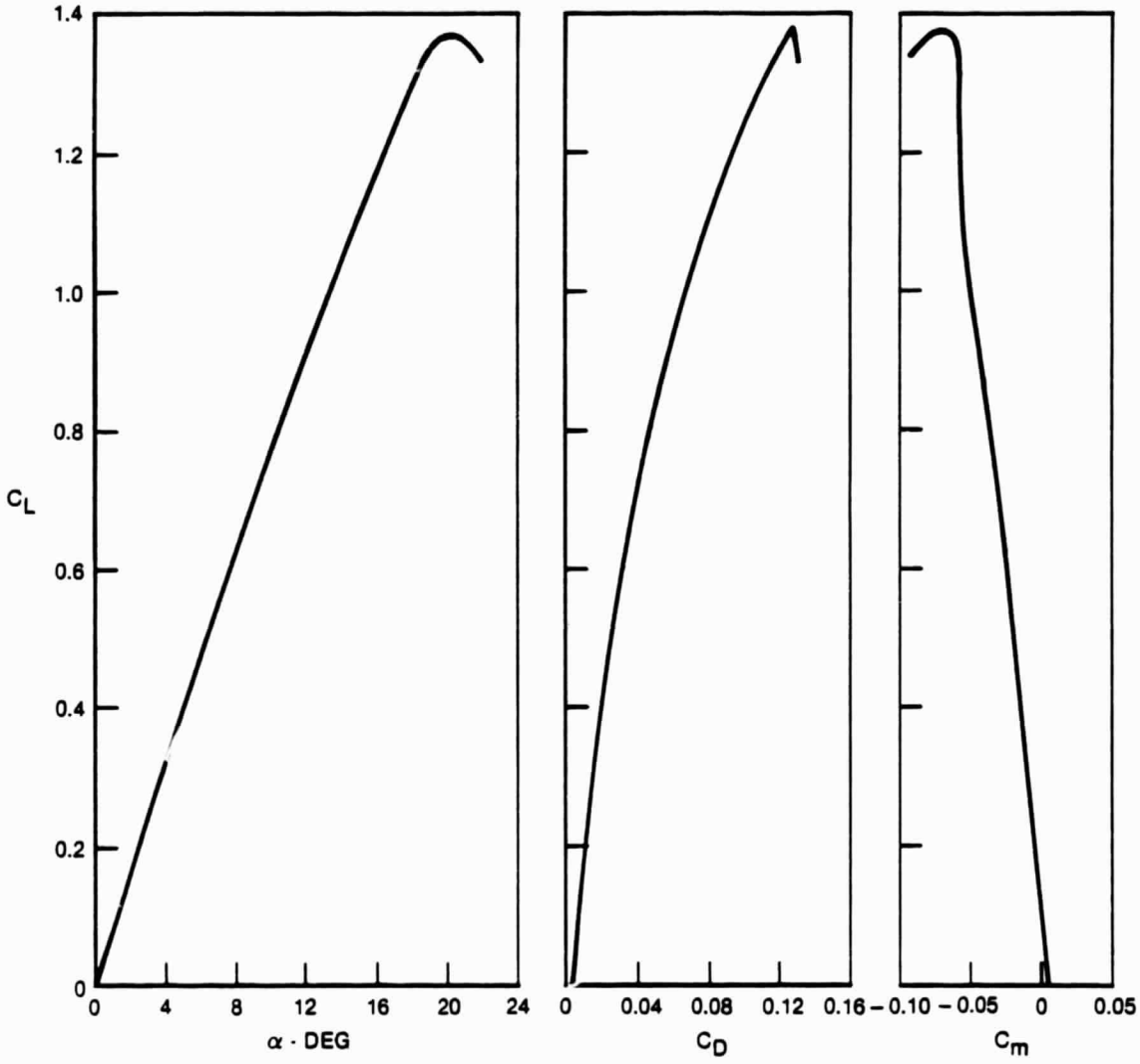

FIGURE 31. NACA 0012, $\Lambda = 20°$, AR = 5.5 FORCE AND MOMENT PREDICTIONS
$R_\infty = 6 \times 10^6$

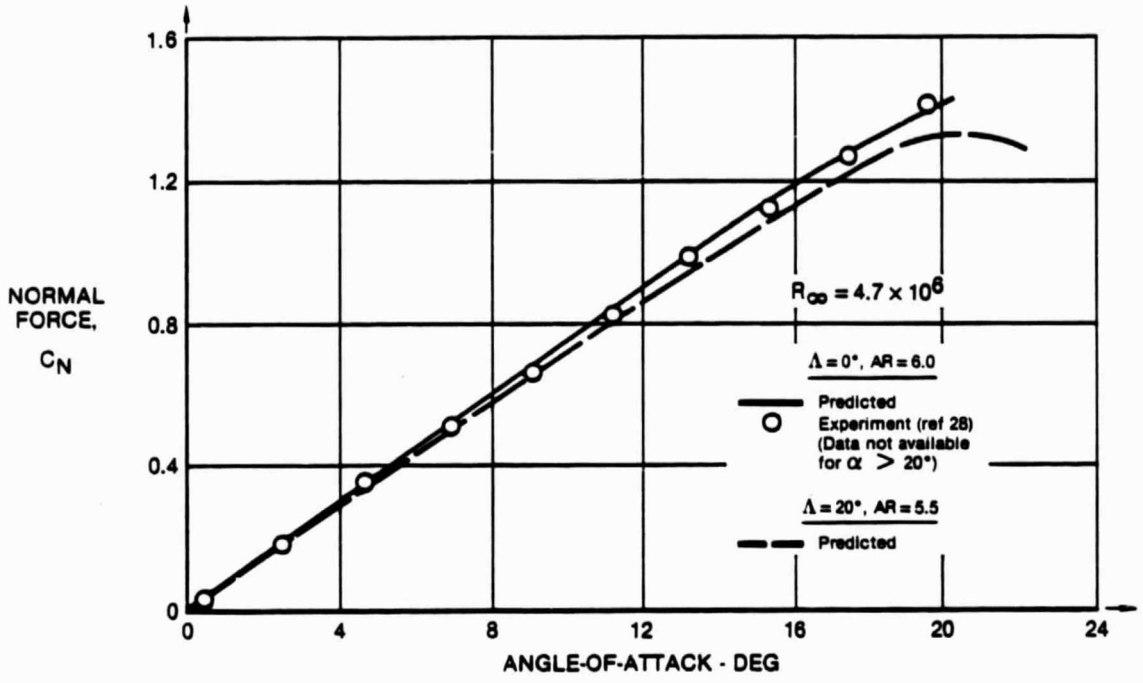

FIGURE 32. COMPARISON OF PREDICTED NORMAL FORCE COEFFICIENT WITH EXPERIMENT FOR WINGS WITH NACA 0012 SECTIONS

NACA 64_1-212 Swept and Tapered Wing

The last wing alone case analyzed was a wing with an aspect ratio of 6, 37.25° leading edge sweep, 0.5 taper ratio, and NACA 64_1-212 sections normal to the leading edge. The geometry is shown in Figure 33. Comparison of predicted forces and pitching moment with experiment are depicted in Figure 34. Separation occurs at an angle-of-attack of twelve degrees. The predictions do not fully account for the detrimental effects of the flow separation. However, comparison of the viscosity included predictions with the viscosity ignored predictions indicate that a substantial portion of the viscous effects are predicted.

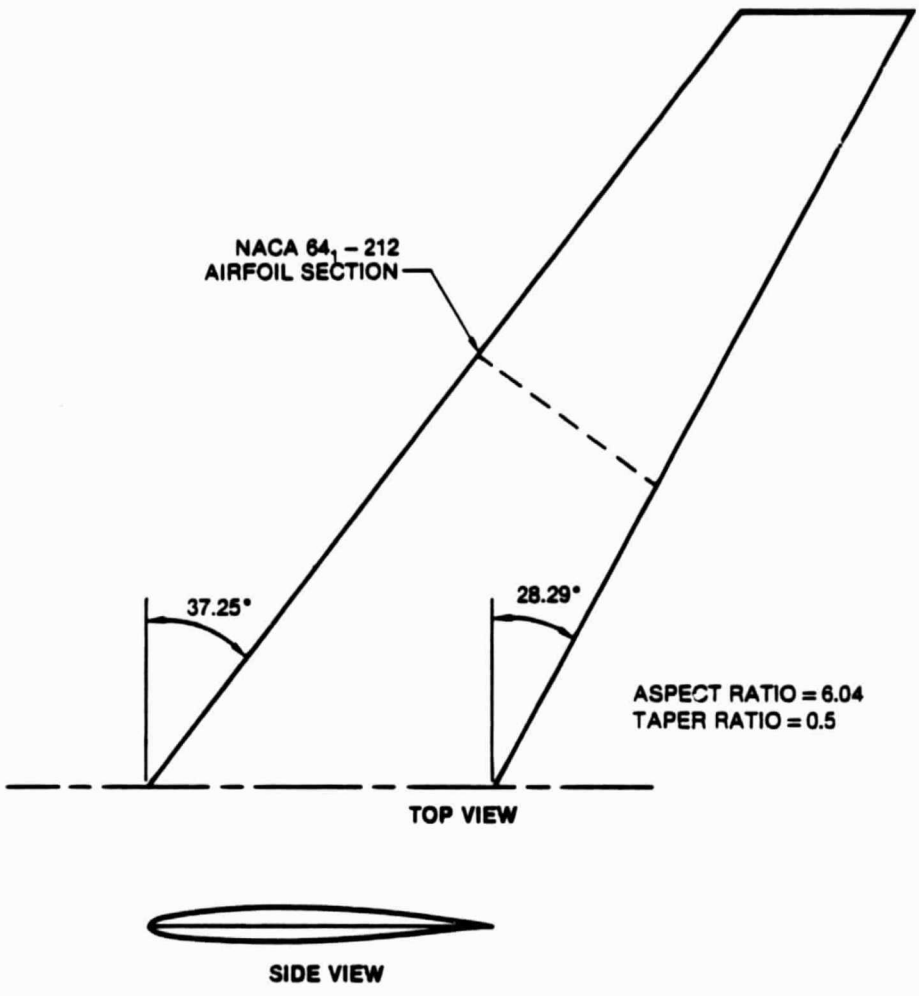

FIGURE 33. GEOMETRY OF SWEPT AND TAPERED WING

YAV-8B Powered Model

The final test case, the YAV-8B powered model, was accomplished to assess the accuracy of the complete jet-airframe interaction method. One of the most important interference effects in V/STOL aerodynamics is the lift increment or decrement due to power effects in the transition flight regime. If the

strong interaction effects are properly modelled, this interference can be accurately predicted.

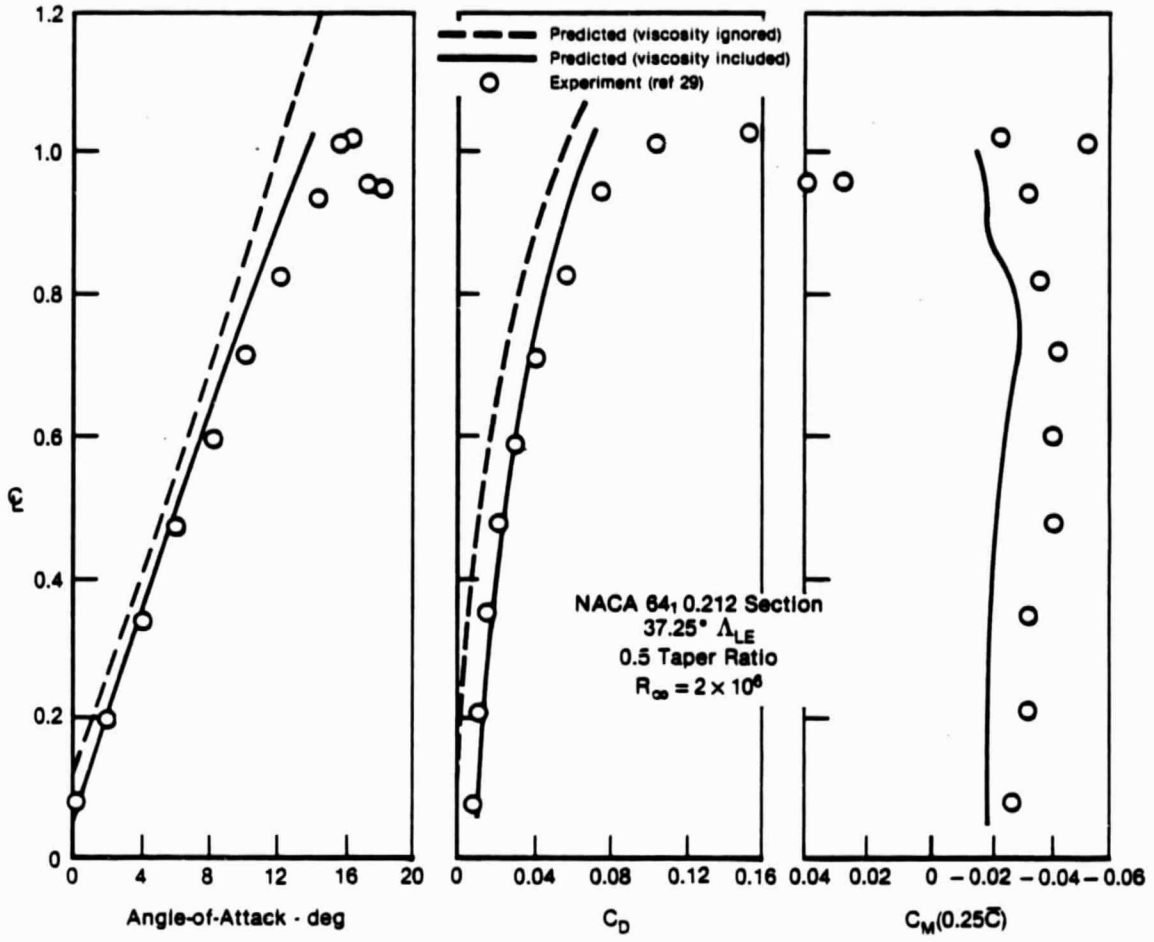

FIGURE 34. COMPARISON OF PREDICTED FORCE AND MOMENT WITH EXPERIMENT FOR A SWEPT AND TAPERED WING

The YAV-8B powered model with flaps deflected 50° was analyzed by the MCAIR jet-airframe interaction method for both power off and power on. Viscous corrections were not included in these calculations due to the presence of part span flaps, which SWAP cannot analyze. The panelled representation of the geometry with jets is shown in Figure 35.

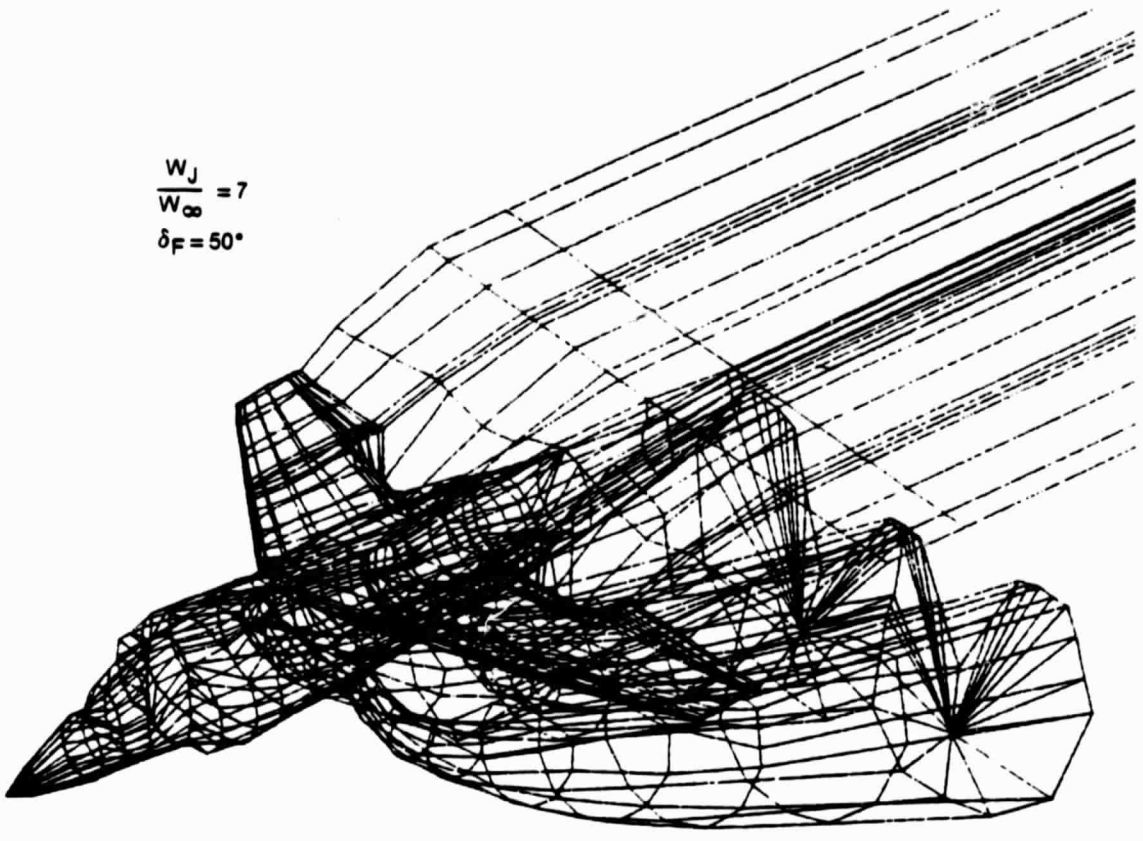

FIGURE 35. PANELED REPRESENTATION OF YAV-8B POWERED MODEL

The predicted lift coefficient at various angles-of-attack is shown in Figure 36 for the YAV-8B with power off. Also shown is the range of experimental data. While the slope of the lift curve is nearly correct, the level is off significantly for not allowing for viscous flow separation on the flap. The ultimate goal of SWAP is to calculate this lift decrement; however, further developments are required.

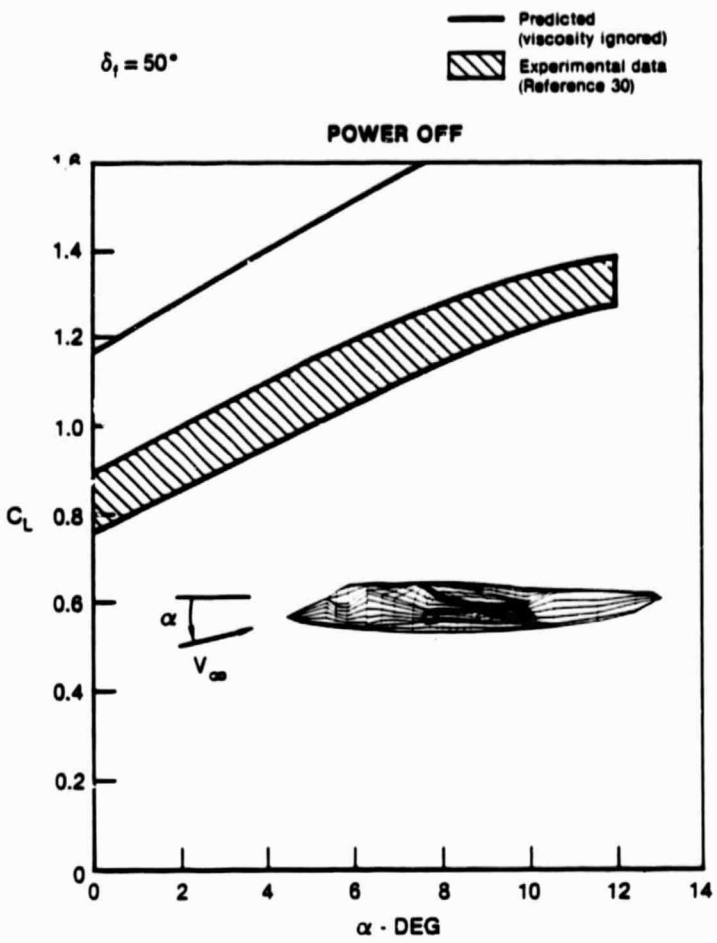

FIGURE 36. YAV-8B POWER OFF

Two different approaches were used to predict the lift coefficient versus angle-of-attack for the YAV-8B with power on (Figure 37). A well designed V/STOL aircraft, such as the YAV-8B, uses the large negative angle-of-attack induced by the jet-entrainment to keep the flow on the flap attached. Thus, an inviscid method should be able to predict the lift curve. The first approach used was to utilize a single calculation of the jet effects at an injection angle corresponding to 0°

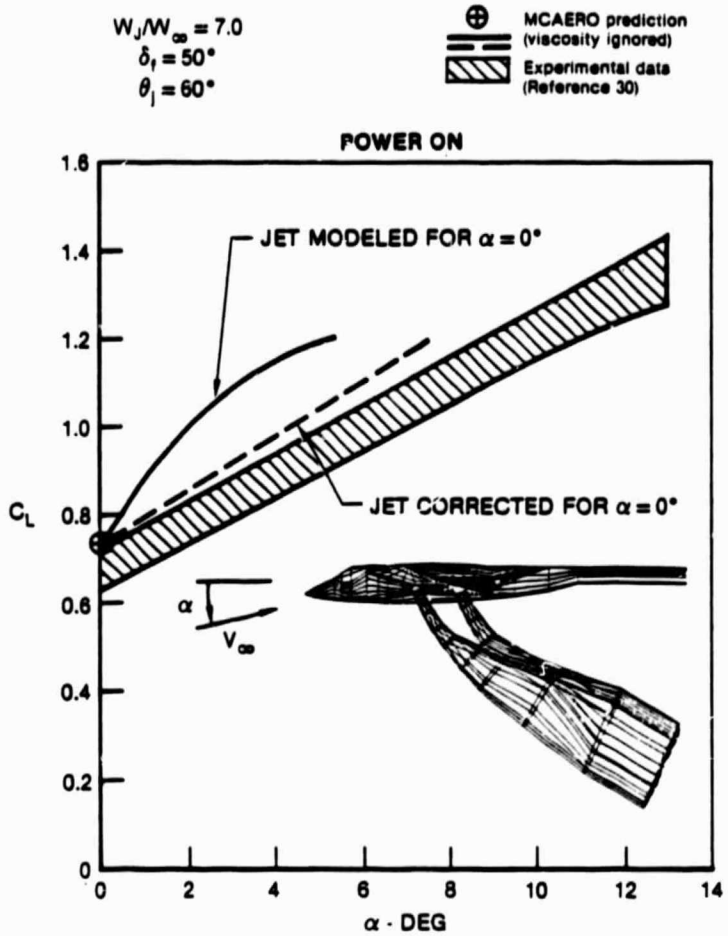

FIGURE 37. AV-8B IN TRANSITION

angle-of-attack. The solid line in Figure 37 is the predicted result. The predicted lift coefficient at 0 ° angle-of-attack is accurate, but the slope of the lift curve is poor. The reason for this descrepancy is that as the angle-of-attack is increased the jet modelling is not correct. A remedy to this would be to recalculate the jet properties at each angle-of-attack. However, an alternative to this expensive procedure is to superimpose the power off calculated slope of the lift curve starting at the predicted lift coefficient at 0° angle-of-attack. This procedure

results in the dotted line in Figure 37, which is quite accurate. The good results are not surprising since the jets act primarily by changing the effective flap deflection, which does not change the slope of the lift curve.

CONCLUSIONS AND RECOMMENDATIONS

The Subsonic Potential Flow Program is accurate and efficient for the analysis of wings, wing-fuselage combinations, and airframe-jet configurations. The Adler-Baron Jet-in-Crossflow Program accurately predicts jet properties for single jets and, when used with the Wooler method for tandem jets, is accurate for multiple jets. The Perturbation Analysis Method accurately predicts inviscid aerodynamic properties for large perturbations in wing geometry characteristic of strong viscous effects. The Stalled Wing Analysis Program, incorporating the Perturbation Analysis Method and the Wing Design Method, correctly accounts for viscous effects for attached flow but has yet to achieve the desired reliability for massive turbulent flow separation on wings and plain wing trailing edge devices. Efforts are continuing to eliminate this deficiency.

The present method utilizes the pilot code of the MCAIR 3-D panel method, which requires an unnecessarily complex set of input parameters. The production version of the MCAIR 3-D panel

method has eliminated the tedious input, and, when used with available graphics technology, the input procedure is very simple. Thus, improvements in the Jet-Airframe-Viscous Interaction Method can be expected when the production version of the MCAIR 3-D panel method is incorporated.

During the course of this investigation several deficiencies were identified in available analytical methods and experimental data. Whereas eliminating these deficiencies represents important research topics, it is beyond the scope of the present effort. These recommended research goals are summarized below.

The Stalled Wing Analysis Program uses a small crossflow laminar boundary layer method and a 2-D empirical correlation for mainflow transition. These methods do not perform well together at high angles-of-attack for swept wings. It is recommended that an improved method for 3-D transition be identified or developed and incorporated into the method. Futhermore, it is recommended that a fully 3-D laminar boundary layer method be tested against the existing method to establish the importance of the crossflow terms within the laminar region. The fully 3-D turbulent boundary layer method used introduces a significant amount of numerical processing and complexity. It is not clear that the crossflow terms are important enough to warrant the complexity. Thus, it is recommended that a small crossflow turbulent boundary layer calculation routine be incorporated into the method and compared with the fully 3-D method.

A search of the literature for experimental data for comparison with prediction indicated some short comings. First, very little pressure data on swept and tapered wings characteristic of modern aircraft were found. Second, pressure data on wings with flaps were not identified. Third, pressure data on wing-fuselage combinations with and without strong jet interactions were scarce. Lastly, detailed pressure data in the wake of jets for realistic configurations were not found. It is recommended that detailed experiments be performed to enlarge the data base to include the identified cases.

REFERENCES

1. Anon., "YAV-8B Aerodynamic Stability and Control Flying Qualities Report", McDonnell Douglas Corporation Report A4637, May 1978.

2. Glaze, L. W., Bristow, D. R., and Kotansky, D. R., "V/STOL Fountain Force Coefficient", NADC-81106-60, Dec 1982.

3. Maskew, B. and Dvorak, F. A., "Investigation of Separation Models for the Prediction of $C_{L_{MAX}}$", Journal of the American Helicopter Society, Vol 23, April 1978, pp. 2-8.

4. Henderson, M. L., "A Solution to the 2-D Separated Wake Modeling Problem and its Use to Predict $C_{L_{MAX}}$ of Arbitrary Airfoil Sections", AIAA Paper 78-156, Jan. 1978.

5. LeBalleur, J. C. and Neron, M., "Cacul D'Ecoulements Visqueux Decolles sur Profils D'Ailes par une Approche de Conplage", AGARD Conference Proceedings, No. 291, Feb 1981, pp. 11-1 to 11-5.

6. Carlson, L. A., "A Direct-Inverse Technique for Low Speed High Lift Airfoil Flowfield Analysis", AGARD Conference Proceedings, No. 291, Feb 1981, pp. 26-1 to 26-10.

7. Gilmer, B. R. and Bristow, D. R., "Analysis of Stalled Airfoils by Simultaneous Perturbation to Viscous and Inviscid Equations", AIAA Journal Vol 20, No. 9, Sept 1982, pp. 1160-1166.

8. Johnson, F. T., "A General Panel Method for the Analysis and Design of Arbitrary Configurations in Incompressible Flow", NASA CR-3079, May 1980.

9. Fray, J. M. and Sloof, J. W., "A Constrained Inverse Method for the Aerodynamic Design of Thick Wings with Given Pressure Distribution in Subsonic Flow", AGARD Conference Proceedings, No. 285, May 1980, pp. 16-1 - 16-9.

10. Malone, J. B., "An Optimal-Surface-Transpiration Subsonic Panel Method for Iterative Design of Complex Aircraft Configurations", AIAA Paper 81-1254, Jun 1981.

11. Hawk, J. D. and Bristow, D. R., "Subsonic Surface Panel Method for Airframe Analysis and Wing Design", AIAA Paper 83-0341, Jan 1983.

12. Bristow, D. R. and Hawk, J. D., "Subsonic Panel Method for the Efficient Analysis of Multiple Geometry Pertrubations", NASA CR 3528, March 1982.

13. Adler, D. and Baron, A., "Prediction of a Three-Dimensional Circular Turbulent Jet in Cross Flow", AIAA Journal, Vol 17, No. 2, Feb 1979, pp. 168-174.

14. Wooler, P. J., "Development of an Analytical Model for the Flow of a Jet into a Subsonic Crosswind", NASA SP-218, Sept 1969.

15. Kamotani, Y. and Greber, V., "Experiments on a Turbulent Jet in a Cross Flow", NASA CR-72893, June 1971.

16. Kellogg, O. D., Foundations of Potential Theory, Dover Publications, Inc., 1953.

17. Bristow, D. R. and Grose, G. G., "Modification of the Douglas Neumann Program to Improve the Efficiency of Predicting Component Interference and High Lift Characteristics", NASA CR-3020, Aug 1978.

18. Morino, Luigi and Kuo, Ching-Chiang, "Subsonic Potential Aerodynamics for Complex Configurations: A General Theory", AIAA Journal, Vol. 12, No. 2, Feb. 1974, pp. 191-197.

19. Fearn, R. L. and Weston, R. P., "Induced Pressure Distribution of a Jet in a Crossflow", NASA TN D-7916, July 1975.

20. Rosenhead, L. (Editor), Laminar Boundary Layers, Clarendon Press. Oxford, 1963, p. 461.

21. Pfenninger, W., "Laminar Flow Control Laminarization", AGARD R-654, March 1977.

22. Smith, P. D., "A Calculation Method for the Turbulent Boundary Layer on an Infinite Yawed Wing in Compressible, Adiabatic Flow", British ARC CP-1268, 1974.

23. Cooke, J. C., "Approximate Calculation of Three-Dimensional Laminar Boundary Layers", British ARC R&M 3201, 1959.

24. Michel, R., as reported in Tani, L., "Boundary Layer Transition", Annual Review of Fluid Mechanics Vol. 1, Annual Reviews, Inc. Palo Alto, 1969.

25. Gross, L. W., "Three-Dimensional Streamline Tracing and Vortex Tracing as Preliminary Steps for the Prediction of the Aerodynamic Characteristics of Aircraft at High Angles of Attack", McDonnell Douglas Corporation Report A3781, Dec. 1975.

26. Smith, P. D., "An Integral Prediction Method for Three-Dimensional Compressible Turbulent Boundary Layers", British ARC R&M 3739, 1974.

27. Pinkerton, R. M., "Calculated and Measured Pressure Distributions Over the Midspan Section of the NACA 4412 Airfoil", NACA Report 562, 1936.

28. Yip, L. P. and Shubert, G. L., "Pressure Distributions on a 1-by 3-Meter Semispan Wing at Sweep Angles from 0° to 40° in Subsonic Flow", NASA TN D-8307, Dec. 1976.

29. Edwards, G. G. and Boltz, F. W., "An Analysis of the Forces and Pressure Distribution on a Wing with the Leading Edge Swept Back 37.25°, "NACA RM A9K01, March 1950.

30. Anon., "AV-8A/B 15% Scale Powered Research and Development Wind Tunnel Tests, Volume I", McDonnell Douglas Corporation Report A3826, Dec. 1975.

APPENDIX I - METRIC COEFFICIENTS

The metric coefficients (h_1, h_2, h_3) establish the relationship between the Cartesian coordinate system (X, Y, Z) and the nonothogonal boundary layer coordinate system (X', Y') on the surface of the wing. The arc length on the surface of the wing, ds, is determined from:

$$ds^2 = h^2{}_1\, dx^2 + h_2{}^2\, dy^2 + h_3{}^2 dxdy \qquad \text{(I-1)}$$

where

$$h_3{}^2 = 2h_1\, h_2 \cos \lambda \qquad \text{(I-2)}$$

and λ is the angle between the X' and Y' axes. These definitions arise out of the use of the metric tensor, which also establishes the relationships between the two coordinate systems:

$$h_1{}^2 = \left(\frac{\partial X}{\partial X'}\right)^2 + \left(\frac{\partial Y}{\partial X'}\right)^2 + \left(\frac{\partial Z}{\partial X'}\right)^2 \qquad \text{(I-3)}$$

$$h_2{}^2 = \left(\frac{\partial X}{\partial Y'}\right)^2 + \left(\frac{\partial Y}{\partial Y'}\right)^2 + \left(\frac{\partial Z}{\partial Y'}\right)^2 \qquad \text{(I-4)}$$

$$h_3 = \frac{\partial X}{\partial X'}\,\frac{\partial X}{\partial Y'} + \frac{\partial Y}{\partial X'}\,\frac{\partial Y}{\partial Y'} + \frac{\partial Z}{\partial X'}\,\frac{\partial Z}{\partial Y'} \qquad \text{(I-5)}$$

Thus, if analytical relationships are known between (X,Y,Z) and (X', Y'), equations (I-3)-(I-5) can be used to calculate h_1, h_2 and h_3.

Consider the wing as broken into two surfaces at the attachment line, and one of these surfaces has been unwrapped and laid flat in a plane. Assume that the unwrapping is accomplished in a way that keeps the lines in the X' direction continuous at the leading edge.

The (X', Y') origin is located at the junction between the wing leading edge and wing root. The functions of Y', a, b, c, and d, are defined as (see Figure A1):

$$a(y') = X'_{ILE}(y') \tag{I-6}$$

$$b(y') = X'_{ATT}(y') - X'_{ILE}(y') \tag{I-7}$$

$$c(y') = X'_{TR}(y') - X'_{ILE}(y') \tag{I-8}$$

$$d(y') = X'_{TE}(y') - X'_{TR}(y') \tag{I-9}$$

From these definitions and by considering the wing to be flat, X, Y, and Z can be determined as:

Laminar Region: $$X = a(y') + b(y') + \left(\frac{a(y')-b(y')}{a(y'=0)-b(y'-0)}\right)(x'-b(y'=o)) \tag{I-10}$$

Turbulent Region: $$X = a(y') + c(y') + \frac{d(y')}{d(y'=0)}(x'-c(y'=0)) \tag{I-11}$$

$$Y = \frac{y'}{(1 + a'^2)^{\frac{1}{2}}} \tag{I-12}$$

$$Z = 0 \tag{I-13}$$

where a' is the derivative of a with respect to y':

$$a' = \frac{da(y')}{dy'} \tag{I-14}$$

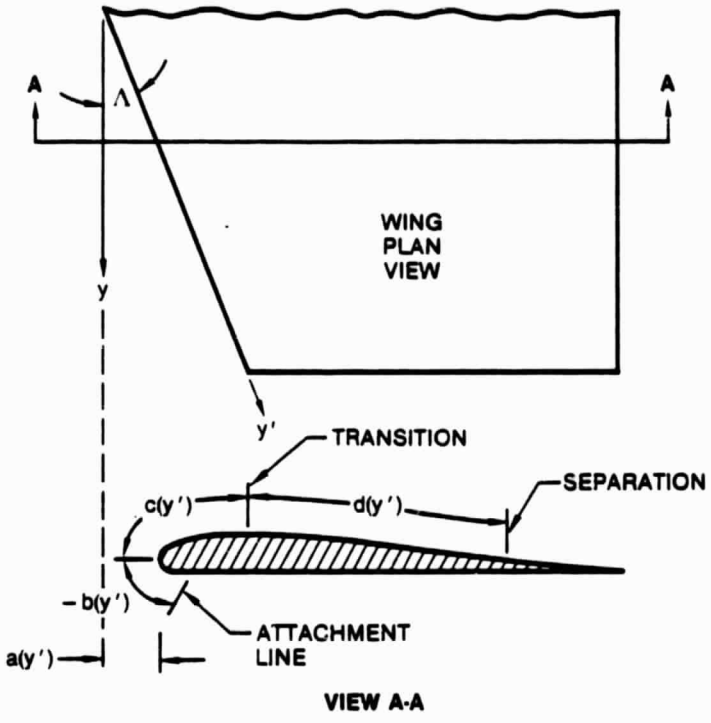

FIGURE A1. DEFINITION OF GEOMETRIC PARAMETERS THAT ESTABLISH METRIC COEFFICIENTS

This definition of Y may seem to be unnecessarily complicated because of the obvious trigonometric relationship between Y and Y'. However, the viscous computation methods require the local value of λ and Y' at each calculation point. Since the region boundaries at each span station are allowed to move independently, these local values can vary from one point to the next.

The angle between the local coordinates, λ_i, is defined as:

$$\tan \lambda_i = \frac{dy'}{dx} \qquad \text{(I-15)}$$

Thus:

$$\text{Laminar Region:} \quad \tan \lambda_i = \frac{1}{a' + b' + \left(\frac{a' - b'}{a(y'=0)-b(y'=0)}\right)(x'-b(y'=0))} \tag{I-16}$$

$$\text{Turbulent Region:} \quad \tan \lambda_i = \frac{1}{a' + c' + \frac{d'}{d(y'=0)}\,(x'-c(y'=0))} \tag{I-17}$$

The metric coefficients h_1, h_2 and h_3 are calculated by differentiating equations (I-10)-(I-13) and substituting into equations (I-3)-(I-5). The results for the turbulent regions are:

$$h_1 = \frac{d(y')}{d(y'=0)} \tag{I-18}$$

$$h_2 = \left[\frac{\left[(a' + c' + \frac{d'}{d(y'=0)}\,(x'-c(y'=0))\right]^2 + 1}{1 + a'^2}\right]^{\frac{1}{2}} \tag{I-19}$$

$$h_3 = \frac{d(y')}{d(y'=0)} \quad \frac{a' + c' + d'/d(y'=0)\,(x'-c'(y'=0))}{(1 + a'^2)^{1/2}} \tag{I-20}$$

The metric coefficients for the laminar regions are not used. The gradients of h_1, h_2, and h_3 in the X' and Y' directions are established by differentiating equations (I-18)-(I-20). Each of the equations presented in this appendix are differentiated with respect to the g_k array for inclusion in the viscous inviscid interaction procedure.